

Fermi National Accelerator Laboratory

FERMILAB-Conf-96/039-E

CDF

**Recent Results in $p\bar{p}$ Collisions at 1.8 TeV from the CDF
Collaboration at the Fermilab Tevatron Collider**

Bruce A. Barnett

For the CDF Collaboration

*Fermi National Accelerator Laboratory
P.O. Box 500, Batavia, Illinois 60510*

*Department of Physics and Astronomy
The Johns Hopkins University
Baltimore, Maryland 21218*

February 1996

Proceedings of the *Conference of the Nuclear and Particle Physics Division of the Russian Academy of Sciences*, Institute of Theoretical and Experimental Physics, Moscow, Russia, October 23-27, 1995

Disclaimer

This report was prepared as an account of work sponsored by an agency of the United States Government. Neither the United States Government nor any agency thereof, nor any of their employees, makes any warranty, expressed or implied, or assumes any legal liability or responsibility for the accuracy, completeness, or usefulness of any information, apparatus, product, or process disclosed, or represents that its use would not infringe privately owned rights. Reference herein to any specific commercial product, process, or service by trade name, trademark, manufacturer, or otherwise, does not necessarily constitute or imply its endorsement, recommendation, or favoring by the United States Government or any agency thereof. The views and opinions of authors expressed herein do not necessarily state or reflect those of the United States Government or any agency thereof.

Recent Results in $p\bar{p}$ Collisions at 1.8 TeV from the CDF Collaboration at the Fermilab Tevatron Collider.

BRUCE A. BARNETT*

Department of Physics and Astronomy
The Johns Hopkins University
Baltimore, Maryland 21218, USA

ABSTRACT

We present recent CDF results on heavy quark physics, electroweak phenomena, quantum chromodynamics, and searches for effects beyond the Standard Model.

1. Introduction

During the 1992-95 Tevatron collider Run I, the Collider Detector at Fermilab (CDF)¹ collected a data sample of $\bar{p}p$ collisions at a center of mass energy of 1.8 TeV with an integrated luminosity of $> 100 \text{ pb}^{-1}$. This was split into two separate data-taking runs: Run 1A ($\sim 20 \text{ pb}^{-1}$) and the present Run 1B ($> 80 \text{ pb}^{-1}$). Data-taking is planned to continue into 1996 and a total sample of about 120 pb^{-1} is expected. This data sample, in combination with improvements to the data acquisition system, the muon coverage, and the installation of the CDF SVX silicon vertex detector,² has allowed many new effects to be studied. This paper reports results on heavy quark (charm, bottom and top) physics, electroweak phenomena, quantum chromodynamics, and searches for new particles beyond the Standard Model.

2. Charm and Bottom Physics

There has been a tremendous number of physics topics studied in the charm and bottom quark sector now that the silicon vertex detector has been incorporated into CDF. These range from measurements of lifetimes of B mesons to production cross sections and searches for rare decays. The discussion here will start by establishing that the individual heavy flavor particles can be identified and their lifetimes can be measured, and then turn to the other measurements like cross sections, etc.

*For the CDF Collaboration; Contribution to the proceedings of the Conference of the Nuclear and Particle Physics Division of the Russian Academy of Science, Institute of Theoretical and Experimental Physics, Moscow, Russia, October 23-27, 1995.

2.1. Mass Measurements

The CDF measurements of the B particle masses³ all rely upon decays through $J/\psi \rightarrow \mu^+ \mu^-$. About 20% of the J/ψ and ψ' events are from B decays so the sample is large. The selected decays are $B^+ \rightarrow J/\psi K^+$, $B^0 \rightarrow J/\psi K^{*0}$, $B_s^0 \rightarrow J/\psi \phi$ and $\Lambda_b \rightarrow J/\psi \Lambda$. Figures (1), (2) and (3) show the relevant mass distributions. The top two parts of (3) show the contributions from events with SVX information and Central Tracking Chamber information separately, while the bottom part is the total signal. Much of the prompt background has been removed by $c\tau$ cuts for these plots. The results are comparable with those from other experiments⁴ as listed below. Here, and throughout this paper, whenever two errors are quoted the first is for statistics and the second is for systematics.

$$\begin{aligned}
 M_{B_u^+} &= 5279.1 \pm 1.7 \pm 1.4 \text{ MeV}/c^2 && (5278.7 \pm 2.0 \text{ (CLEO)}) \\
 M_{B_d^0} &= 5281.9 \pm 2.2 \pm 1.4 \text{ MeV}/c^2 && (5279.0 \pm 2.0 \text{ CLEO}) \\
 M_{B_s^0} &= 5369.9 \pm 2.3 \pm 1.3 \text{ MeV}/c^2 && (5368.5 \pm 5.3 \text{ (LEP ave)}) \\
 M_{\Lambda_b} &= 5623 \pm 5 \pm 4 \text{ MeV}/c^2 && (5621 \pm 17 \pm 15 \text{ ALEPH})
 \end{aligned}$$

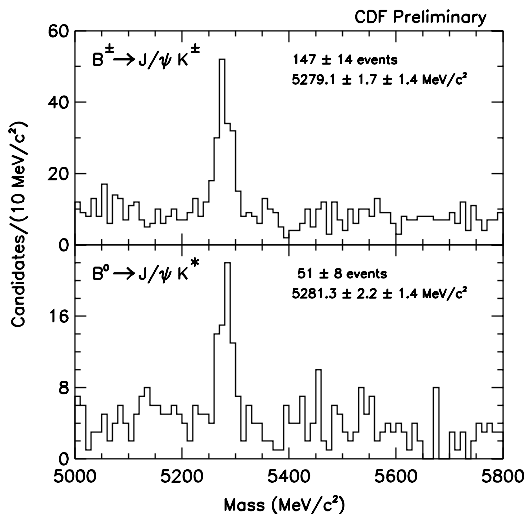


Figure 1: $B^\pm \rightarrow J/\psi K^\pm$ (top) and $B^0 \rightarrow J/\psi K^{*0}$ (bottom) invariant mass distributions from Run 1A.

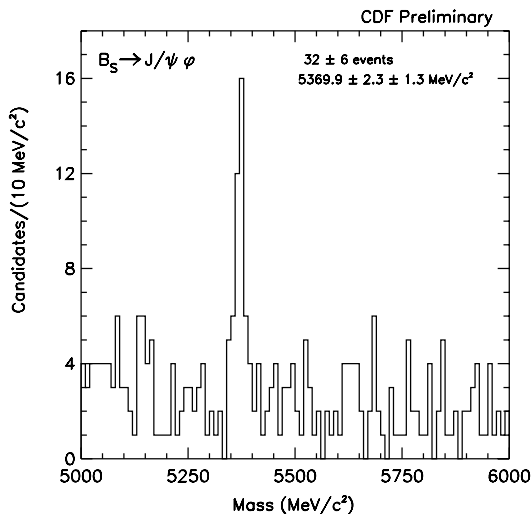


Figure 2: $B_s^0 \rightarrow J/\psi \phi$ invariant mass distribution from Run 1A.

2.2. B Meson Lifetimes

Measurements of the lifetimes of heavy quark particles are important for testing the predictions of lifetimes from the Heavy Quark Effective Theory (HQET) calculations and for understanding the relative contributions from non-spectator decays. Only a small difference is expected between the lifetimes of B_u^+ , B_d^0 and B_s^0 mesons. For the

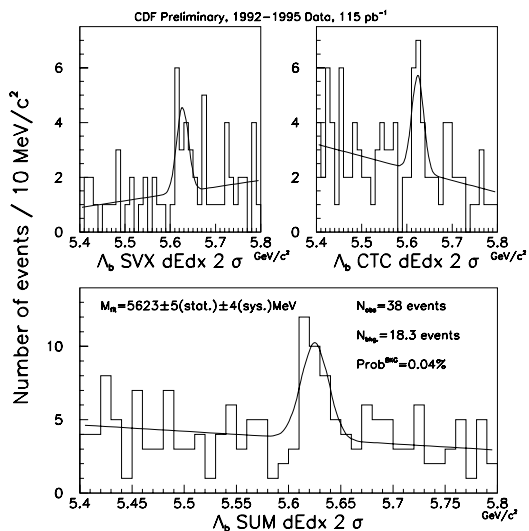


Figure 3: $\Lambda_B \rightarrow J/\psi \Lambda$ invariant mass distribution.

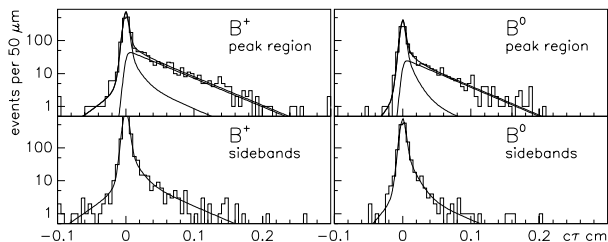


Figure 4: The proper lifetime distributions for B^+ and B^0 from the exclusive decay channels (top) and for the sideband mass regions (bottom).

B_u^+ and B_d^0 the difference might be $\sim 5\%$.⁵ CDF can measure these lifetimes via two complimentary techniques: fully reconstructed exclusive decays⁶ and more loosely defined inclusive decays. For the B_s^0 it has been suggested that the lifetimes for the two CP eigenstates produced through mixing of the B_s and the \bar{B}_s may differ by as much as 20%.⁷ Such an effect would show up as a difference between the B_s semileptonic decay, which is a mixture of the two CP eigenstates, and the decay of $B_s \rightarrow J/\psi \phi$, which is supposed to be mainly CP even.

For the lifetime measurement of $B_{u,d}$ through fully reconstructed exclusive decays CDF uses the decay modes $B \rightarrow \Psi^X K^X$, where Ψ^X is either J/ψ or ψ' and K^X is K^\pm , $K_s^0 \rightarrow \pi^+ \pi^-$, $K^*(892)^\pm \rightarrow K_s^0 \pi^\pm$ or $K^*(892)^0 \rightarrow K^\mp \pi^\pm$. No cut on the $c\tau$ of the event is made for the lifetime analysis, unlike the mass analysis. The decay length in the transverse plane, L_{xy} , is the projected distance between the primary and secondary vertices. The proper decay length is calculated as $c\tau = L_{xy} \times M(B)/P_T(B)$ where $M(B)$ is the meson's mass and $P_T(B)$ is the meson's transverse momentum. B meson candidates are required to have a mass difference $|\Delta M| < 30 \text{ MeV}/c^2$ with respect to the world average. The background shape is determined using the sideband regions of $60 \text{ MeV}/c^2 \leq |\Delta M| \leq 120 \text{ MeV}/c^2$. The $c\tau$ data are shown in Figure (4).

For the lifetime measurement using an inclusive signal, CDF has reconstructed charmed mesons from semileptonic B decays. The selected charm decay modes, along with corresponding charge conjugates, were:

$$\begin{aligned}
& D^0 \rightarrow K^- \pi^+ \\
& D^{*+} \rightarrow D^0 \pi^+ \quad D^0 \rightarrow K^- \pi^+ \\
& D^{*+} \rightarrow D^0 \pi^+ \quad D^0 \rightarrow K^- \pi^+ X \\
& D^{*+} \rightarrow D^0 \pi^+ \quad D^0 \rightarrow K^- \pi^+ \pi^+ \pi^-
\end{aligned}$$

Here $c\tau = L_{xy} \times M(B) \times K / P_T(B)$ where K is a Monte Carlo derived average correction factor due to the partial B reconstruction. One of the sets of $c\tau$ data, $B^+ \rightarrow lD^0 X$, $D^0 \rightarrow K^- \pi^+$, is shown in Figure (5). The dotted curve comes from the sideband data.

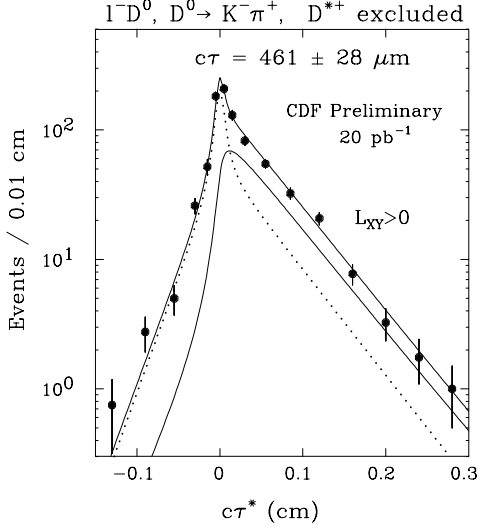


Figure 5: The pseudo $c\tau$ distribution for $B^+ \rightarrow lD^0 x$, $D^0 \rightarrow K^- \pi^+$.

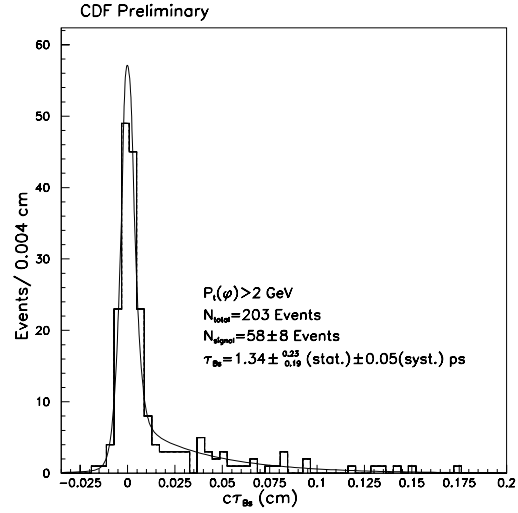


Figure 6: The proper lifetime distribution for $B_S^0 \rightarrow J/\psi\phi$

The lifetime of the B_S^0 meson was also measured in the exclusive and inclusive manner.⁸ The exclusive method fully reconstructed the $B_S^0 \rightarrow J/\psi\phi$ decay. For the Run 1A and Run 1B data there were 58 events. The proper lifetime distribution for the exclusive decay analysis is shown in Figure (6). The inclusive method utilized the partially reconstructed channel $B_S^0 \rightarrow D_S l \nu$, $D_S \rightarrow \phi\pi$ with 19.3 pb^{-1} of data.

The results of all of these lifetime measurements are:

$$\begin{aligned}
\tau_{B_u^+} &= 1.68 \pm 0.09 \pm 0.06 \text{ psec} \quad (J/\psi K) \\
&= 1.51 \pm 0.12 \pm 0.08 \text{ psec} \quad (D^* l) \\
\tau_{B_d^0} &= 1.64 \pm 0.11 \pm 0.06 \text{ psec} \quad (J/\psi K) \\
&= 1.57 \pm 0.08 \pm 0.07 \text{ psec} \quad (D^* l) \\
\frac{\tau_{B_u^+}}{\tau_{B_d^0}} &= 1.02 \pm 0.09 \pm 0.01 \quad (\psi K) \\
&= 0.96 \pm 0.10 \pm 0.05 \quad (D^* l) \\
&= 1.00 \pm 0.07 \quad (\text{combined})
\end{aligned}$$

$$\begin{aligned}
\tau_{B_s^0} &= 1.34_{-0.19}^{+0.23} \pm 0.05 \text{ psec} \quad (J/\psi\phi) \\
&= 1.42_{-0.23}^{+0.27} \pm 0.11 \text{ psec} \quad (D_s l\nu, D_s \rightarrow \phi\pi)
\end{aligned}$$

2.3. Charmonium Production

Charmonium states can be produced by a variety of mechanisms in $p\bar{p}$ collisions. The J/ψ 's and $\psi(2S)$'s come from direct production or from b hadron decay. Additionally, J/ψ 's can be produced in radiative decays of χ_c mesons. The χ_c mesons can be produced directly or from b hadron decays.

The differential and integrated production cross sections for J/ψ and $\psi(2S)$ were measured using 15.5 and 18 pb^{-1} of data, respectively.⁹ Both particles were identified via their dimuon decay mode with $P_T > 4 \text{ GeV}/c$ and $|\eta| < 0.6$. The silicon vertex detector information allowed reconstruction of the $\mu^+\mu^-$ vertex, which could then be classified as either prompt or secondary. The secondary decays are assumed to come from B decays. Figure (7) displays the prompt, non-prompt and total production cross sections for $\psi(2S)$ versus P_T along with the theoretical predictions. There is reasonable agreement between the data and theory for the production from the non-prompt B decays but the prompt production is much larger in the data than theory, about a factor of 50! The differential cross section for the J/ψ shows a similar effect. There has been much theoretical speculation regarding the explanation of this discrepancy.¹⁰

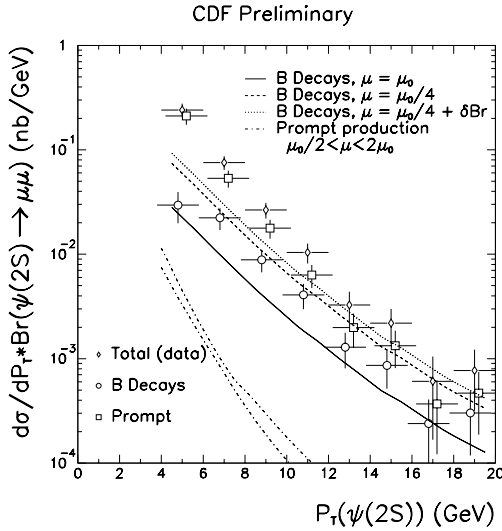


Figure 7: The prompt and non-prompt differential cross section for $\psi(2S)$ versus P_T along with the theoretical predictions.

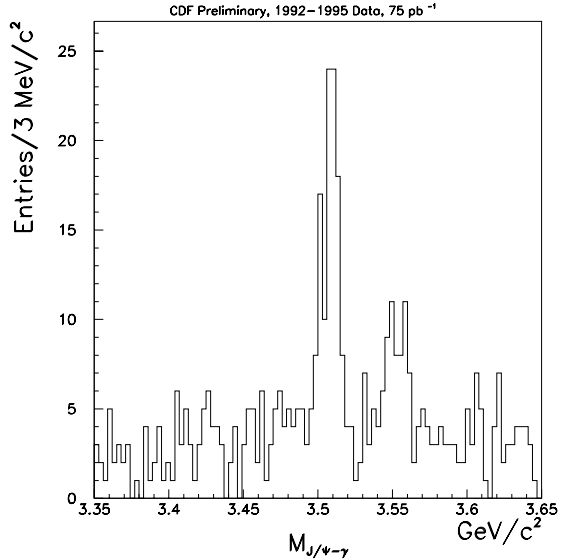


Figure 8: χ states reconstructed from the mass difference $M(\mu^+\mu^-\gamma) - M(\mu^+\mu^-)$ in the J/ψ region with $P_T^\gamma > 1 \text{ GeV}/c$.

CDF first saw the charmonium p states, the χ 's, through the channel $\chi \rightarrow J/\psi\gamma$, $J/\psi \rightarrow \mu^+\mu^-$ with the γ being identified in the electromagnetic calorimeter.¹¹ The energy resolution was not sufficient to separate the different χ states using this method,

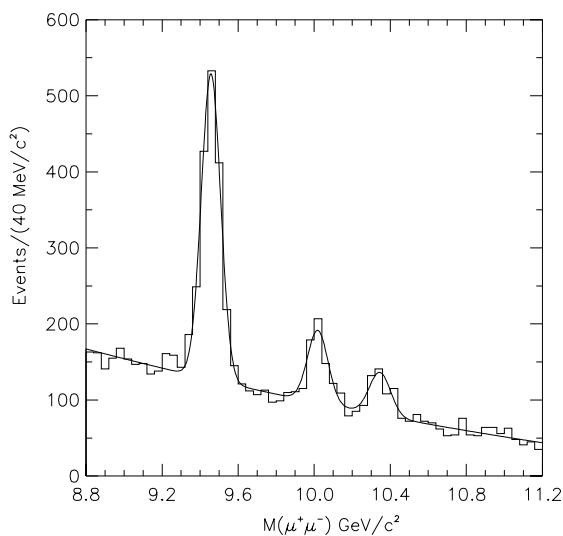


Figure 9: $\Upsilon \rightarrow \mu\mu$ mass states.

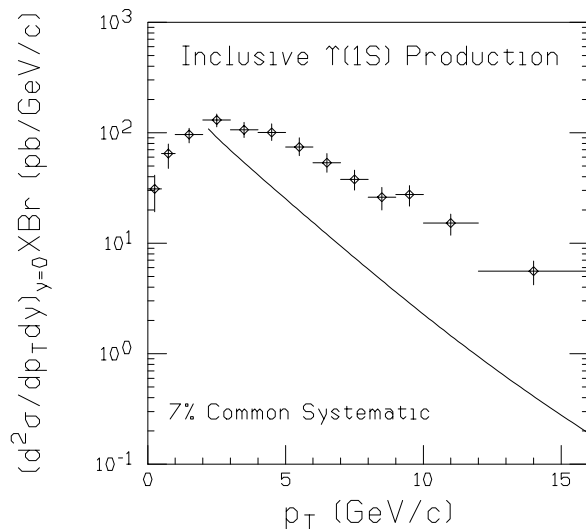


Figure 10: Υ (1S) production cross section vs. P_T .

but the efficiency was reasonably high. The present analysis has 75 pb^{-1} of data and uses γ conversions in the inner CDF material. This efficiency is lower but the energy resolution enables the isolation of the individual states, as shown in Figure (8). There are 46.4 ± 7.2 prompt χ_1 's and 23.2 ± 6.4 prompt χ_2 's. The prompt signal is defined by having the proper decay distance of the $J/\psi\gamma$ system be less than $100 \mu\text{m}$. Incorporating the relative detection efficiencies gives the ratio of production cross sections as:

$$\frac{\sigma(\chi_2)}{\sigma(\chi_1)+\sigma(\chi_2)} = 0.47 \pm 0.08 \pm 0.02.$$

2.4. Bottomonium Υ Production

In a manner similar to the identification of J/ψ , CDF has identified the $b\bar{b}$ bound states, the Υ 's, via $\Upsilon \rightarrow \mu^+\mu^-$. In 16.6 pb^{-1} of data there are 1,248 $\Upsilon(1S)$, 300 $\Upsilon(2S)$ and 203 $\Upsilon(3S)$ events in the rapidity range $|y| < 0.4$ as shown in Figure (9). The production rates are higher than expected by factors of about 3 for $\Upsilon(1S)$ and $\Upsilon(2S)$ and about 10 for $\Upsilon(3S)$. Figure (10) shows the cross section versus P_T for the $\Upsilon(1S)$. The theoretical curve is a leading order calculation generated using MRSD0 PDF and scale $\mu^2 = P_T^2 + m_\Upsilon^2$. There is significant theoretical work¹² underway to clarify this discrepancy.

2.5. B Meson Production

CDF has measured the B meson production cross section for inclusive decay channels as well as exclusive decay channels. The inclusive decay channels contain leptons, J/ψ , ψ' and/or charm. The exclusive channels are those described above for the B meson mass measurements: $B^\pm \rightarrow J/\psi K^\pm$ and $B^0 \rightarrow J/\psi K^{*0}$, $K^{*0} \rightarrow K^+\pi^-$. The measurements are based upon 19.3 pb^{-1} of data. The cross sections are shown in

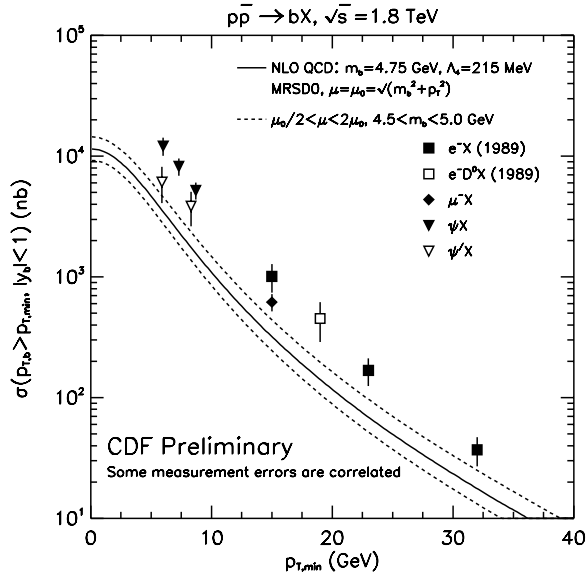


Figure 11: Integral cross section for b production

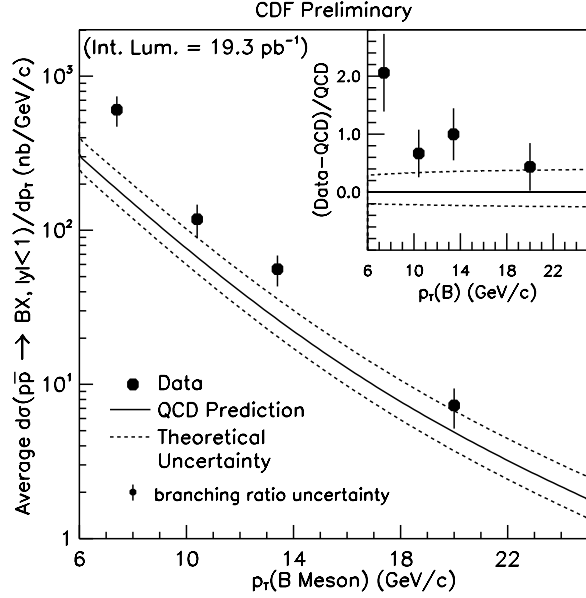


Figure 12: Exclusive differential cross section for B production.

Figures (11) and (12) along with the NLO calculation of Nason, Dawson and Ellis¹³ convoluted with the Peterson fragmentation.¹⁴ The data in both figures lie somewhat above the theory.

It is important to be able to examine the correlations between the b and \bar{b} quark production to check theoretical models and the B meson production just discussed. The exclusive and inclusive B meson identification is not efficient enough to use for correlation studies. CDF utilizes the fact that muons produced by the decay of particles containing a b quark will tend to have a larger impact parameter relative to the primary vertex than muons from other sources. For example, the b quark lifetime is larger than the c quark lifetime. Since the tail of the muon impact parameter distribution includes muons from b , c and other background, the data must be fit by a sum of contributions. After corrections for efficiencies and acceptances, CDF obtains the $b - \bar{b}$ correlated cross section shown in Figure (13). One of the b 's must have $P_T(b) \geq 6.5$ GeV/c, with $|y_b| \leq 1.0$, while the second b can have a variable transverse momentum as $P_T(\bar{b}) \geq P_T^{min}$, $|y_{\bar{b}}| \leq 1.0$. The data are higher than the NLO calculations¹⁵ by a factor of nearly 3, similar to the effect seen earlier in the B or b cross section.

2.6. Rare B Decays

Because the B production cross section is so large, $p\bar{p}$ collisions are a good laboratory for searching for rare B decays. CDF has limits on the decays $B \rightarrow \mu\mu K$, where K can be either K^\pm or K^{*0} , and on $B \rightarrow \mu\mu$. All of these decays are suppressed in the

CDF Preliminary

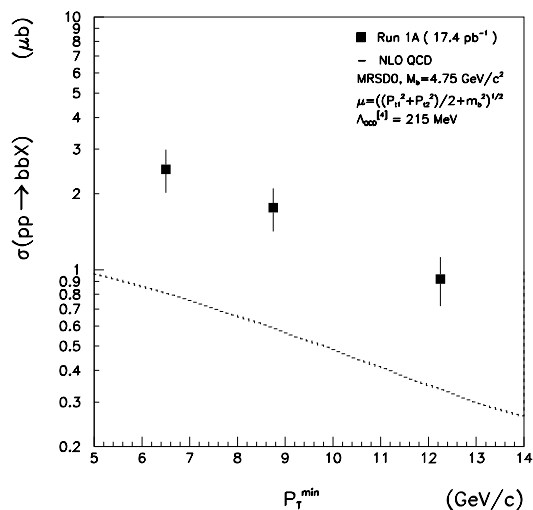


Figure 13: b-b Correlated Cross Section from $\mu\mu$ production.

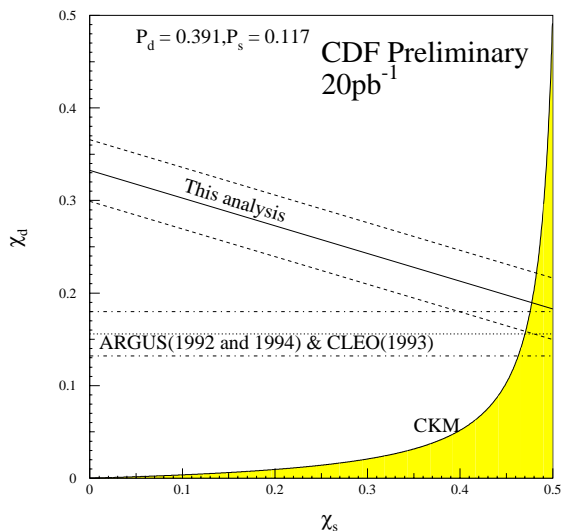


Figure 14: The mixing parameter for B_d versus that for B_s from time integrated $e\mu$ measurement. The bands represent 1σ uncertainties.

Standard Model¹⁶ so unusually large rates could indicate physics beyond the SM. The CDF 90% C.L. limits are

$$\begin{aligned} \text{BR}(B^\pm \rightarrow \mu\mu K^\pm) &< 1.1 \times 10^{-5}, \\ \text{BR}(B^0 \rightarrow \mu\mu K^*) &< 2.1 \times 10^{-5}, \\ \text{BR}(B_d \rightarrow \mu\mu) &< 1.6 \times 10^{-6} \\ \text{and } \text{BR}(B_s \rightarrow \mu\mu) &< 8.4 \times 10^{-6}. \end{aligned}$$

While these are the world's most sensitive limits, they are still about 2 orders of magnitude above the SM predictions.

2.7. B Mixing

CDF data from the SVX allows $B^0\bar{B}^0$ mixing to be studied via both the time integrated and time dependent approach. In both cases the flavor of the b is determined from the sign of the lepton, e or μ , in the semileptonic decay $b \rightarrow l^+ + c$ and $\bar{b} \rightarrow l^- + \bar{c}$.

No separation of the contributions from B_d vs. B_s is made for the time integrated mixing measurement. Therefore, the mixing parameter, defined as

$$\chi = \frac{B \rightarrow \bar{B}}{(B \rightarrow B) + (B \rightarrow \bar{B})} = P(B^0 \rightarrow \bar{B}^0) = \int_0^\infty | \langle \bar{B}^0 | B^0 \rangle |^2 dt,$$

is a mixture of the various mixing parameters, $\bar{\chi} = F_d \chi_d + F_s \chi_s$, where the F 's are the average fractions of B_d and B_s . This χ parameter can also be expressed in terms of the neutral B mass splitting and the B total width as

$$\chi = \frac{x^2}{2(1+x^2)} \text{ where } x \equiv \Delta m / \Gamma = \tau \Delta m.$$

CDF measures the number of like-sign (LS) vs. opposite-sign (OS) lepton pairs:

$$R = \frac{(LS)}{(OS)} = \frac{2\bar{\chi}(1-\bar{\chi}) + (\bar{\chi}^2 + (1-\bar{\chi})^2)f_s}{\bar{\chi}^2 + (1-\bar{\chi})^2 + 2\bar{\chi}(1-\bar{\chi})f_s + f_c},$$

where f_s is the sequential decay fraction and f_c is the charm fraction from $c\bar{c}$ production. For the case where an electron and muon is identified, $\bar{\chi} = 0.118 \pm 0.008 \pm 0.020$ and for the case where two muons are identified $\bar{\chi} = 0.136 \pm 0.028 \pm 0.022$. Figure (14) shows the result for the $e\mu$ case.

The time dependent mixing measurement uses secondary vertex tagging in the dimuon data sample. A secondary vertex is required of one μ and at least 2 other tracks. The tracks, excluding the μ , are required to be consistent with a D decay. Figure (15) shows the like sign fraction versus pseudo $c\tau$. The best fit to the data gives $x_d = \Delta m / \Gamma = 0.64 \pm 0.18 \pm 0.21$ or $\Delta m_d = 0.44 \pm 0.12 \pm 0.14 \text{ psec}^{-1}$.

3. Observation of Top Quark Production

The top quark is required to exist in the Standard Model as the weak isospin partner of the bottom quark. The first direct evidence for $t\bar{t}$ production in $p\bar{p}$ collisions was presented by CDF in April 1994¹⁷ based upon 19.7 pb^{-1} of data. In March 1995 CDF¹⁸ and D0¹⁹ both announced the observation of the top quark, confirming the 1994 CDF evidence. CDF has also presented evidence for the top quark in subsequent publications using additional analysis techniques.²⁰ CDF now has about 100 pb^{-1} of data for its top analyses.

At CDF top quarks are expected to be produced in pairs primarily by $q\bar{q}$ annihilation with only a small contribution from gg fusion. The top quarks should then decay into a real W boson and a b quark for $M_{top} > M_W + M_b$. The production and decay process is shown in Figure (16). The final event topology is determined by the decay modes, (W \rightarrow lepton + neutrino) or (W \rightarrow quark + antiquark), of the two final state W bosons. Ignoring the (W \rightarrow tau + neutrino) decay, the events can be classified as having 0, 1, or 2 final state electrons and muons. The CDF analyses concentrated on three channels:

- Dilepton Channel. About 5% of the time the W decays produce two high P_T electrons or muons associated with two b jets and large missing energy due to the missing neutrinos. This is the cleanest final state because it has a signal to background of about 4.

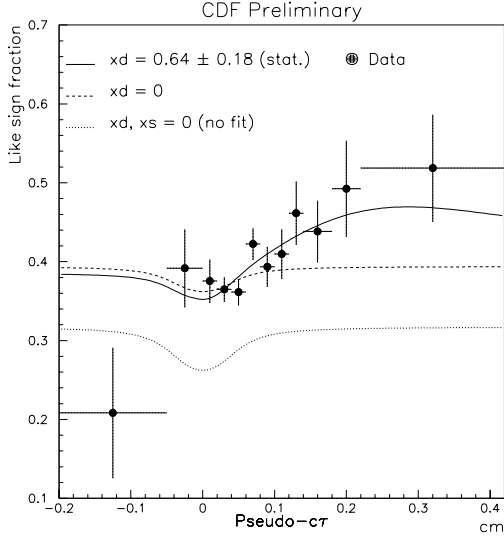


Figure 15: Like sign μ fraction versus $c\tau$. The solid line is the fit to the data. The dashed line is the fit after forcing $x_b = 0.0$ and the dotted line is the prediction for only the sequential decay contribution and both x_b and $x_s = 0.0$.

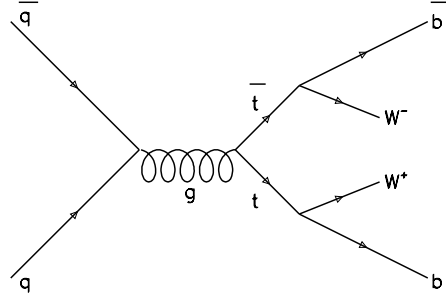


Figure 16: Standard Model production and decay of $t\bar{t}$ quarks.

- **Single Lepton Plus Jets:** About 30% of the time the W decays produce one high P_T electron or muon and two $q\bar{q}$ jets all associated with two b jets and missing neutrinos, i.e. the final state is one high P_T lepton, four jets and \cancel{E}_T . The background comes mainly from the production of W bosons along with low mass quark jets. The signal to background is about 0.2, which means additional requirements are needed to isolate the top quark signal. CDF suppresses the W plus multijet background by requiring evidence of b jets in the event. Two techniques are utilized. The first, and more powerful, utilizes the Silicon Vertex Detector, SVX, to identify decay vertices of b hadrons separated from the original interaction point. This isolation of the secondary decay is possible because of the “long” lifetime of the b quark, ~ 1.3 psec, $c\tau \sim 450$ microns. The second technique, called the semileptonic tag or SLT, searches for the lower momentum leptons (e or μ) from the semileptonic decay of the b hadrons.

- All Hadronic State: About 44% of the time both W bosons decay into $q\bar{q}$ jets. Including the two b jets this gives a six jet final state. There is a huge background from other QCD multijet processes giving a signal to background for top of about 0.01. Analysis of this channel was too difficult for inclusion in any previous CDF publications, but now some confirming evidence of top quark production is becoming visible.

The discussion here will cover the “counting experiments” of looking for evidence for top in the first two of the above three channels. Then the calculation of the production cross section and mass will be described. During this discussion various pieces of confirming kinematic evidence will be presented.

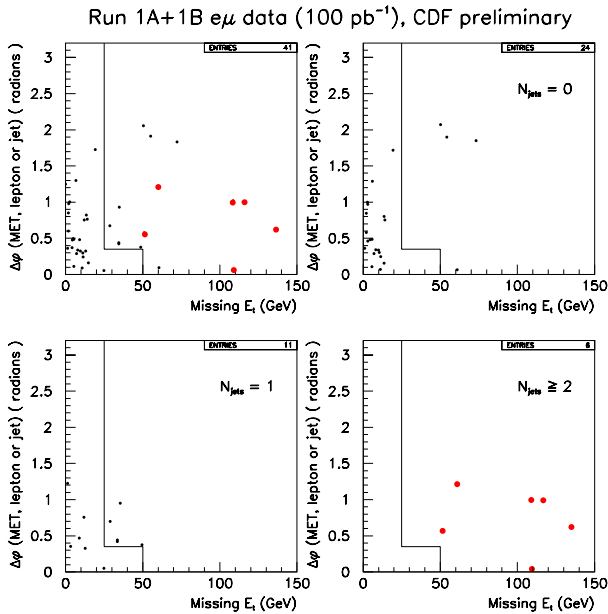


Figure 17: \cancel{E}_T vs. $\Delta\phi$ between the \cancel{E}_T vector and the nearest jet or lepton.

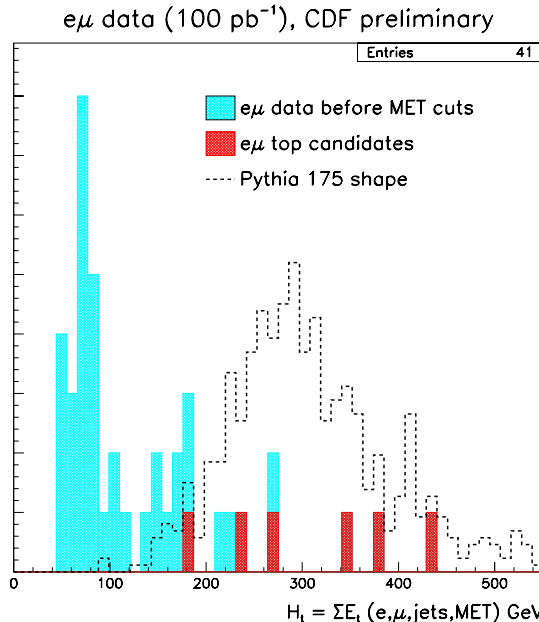


Figure 18: Total transverse energy of $e\mu$ dilepton events.

3.1. Observation of Top Production in the Counting Experiments.

The analyses for the two counting experiments, dilepton and single lepton plus jets, look for an excess of events relative to the known, expected backgrounds. Both analyses begin with the high P_T inclusive e/μ samples. These have $E_T^e > 20$ GeV or $P_T^\mu > 20$ GeV/ c with $|\eta| < 1.0$. For events with a second lepton if the M_{e+e-} or $M_{\mu+\mu-}$ is between 75 and 105 GeV/ c^2 the event is removed as a possible Z boson decay.

3.1.1. Dilepton Channel

Several additional cuts are made on events with two leptons to remove backgrounds. To remove Drell-Yan events the magnitude of \cancel{E}_T is required to be at least 25 GeV. If the \cancel{E}_T is less than 50 GeV the azimuthal angle between the \cancel{E}_T vector and the nearest jet or lepton is required to be larger than 20° to avoid effects of mismeasurement of jet or lepton energies. Lastly, all events must have at least two jets with E_T greater than 10 GeV and $|\eta| < 2.0$. Figure (17) shows the events versus these variables for the case where there is an $e\text{-}\mu$ dilepton pair and various numbers of jets.

A total of 9 events survive these cuts: 1 ee , 2 $\mu\mu$, and 6 $e\mu$. The relative acceptances for these three modes are 15%, 28% and 57%, respectively. The estimated background from radiative Z decay is expected to contribute less than 0.1 event, but one of the $\mu\mu$ events includes an energetic photon which forms an invariant mass with the two muons, $M_{\mu\mu\gamma}$, of 86 GeV/ c^2 . Since this is very close to M_Z it is removed to be conservative. This leaves 8 events. The total expected background is 1.9 ± 0.4 events. The probability of this background fluctuating to 8 events is about 10^{-3} .

There is additional strong evidence that most of these events are from top production. Three of the events contain a total of five SVX or SLT b-tags giving strong evidence for WWb. Also, the total transverse energy, $H_T = \Sigma E_T(e, \mu, jets, \cancel{E}_T)$, can be compared to what would be expected from backgrounds and top, as in Figure (18) for the $e\mu$ events. The H_T for the data clearly resembles the production of both top and background more than just background.

3.2. Lepton Plus Jets Channel

The search for top production in the lepton (e, μ) plus jets channel begins with the standard lepton plus jets sample and adds several cuts: 1) lepton $E_T > 20$ GeV, 2) $\cancel{E}_T > 20$ GeV, and 3) at least 3 jets with $E_T > 15$ GeV and $|\eta| < 2.0$. Although about 30% of top events should be in this channel the signal to background would be about 0.2. Thus, additional cuts are required to isolate top. These cuts look for evidence of b quark jets. The most powerful method, the SVX tag, searches for the secondary decay vertex of the $b(\bar{b})$ quark using the silicon vertex detector. It has an efficiency of $42 \pm 5\%$. The second method, the SLT tag, searches for an additional lepton from the semileptonic b decay. It has an efficiency of $20 \pm 2\%$.

SVX b-TAGGING	TOTAL BACKGROUND	OBSERVED TAGS
W + 1 Jet	74.5 ± 16.9	61 (61)
W + 2 Jets	29.7 ± 7.9	43 (38)
W + ≥ 3 Jets	9.9 ± 2.8	40 (32)
SLT b-TAGGING		
W + 1 Jet	250 ± 38	232 (229)
W + 2 Jets	71 ± 11	84 (83)
W + ≥ 3 Jets	23.8 ± 3.6	40 (36)

TABLE 1: Backgrounds and number of tags for SVX and SLT

Table 1 compares the data for the number of tagged jets and the number of

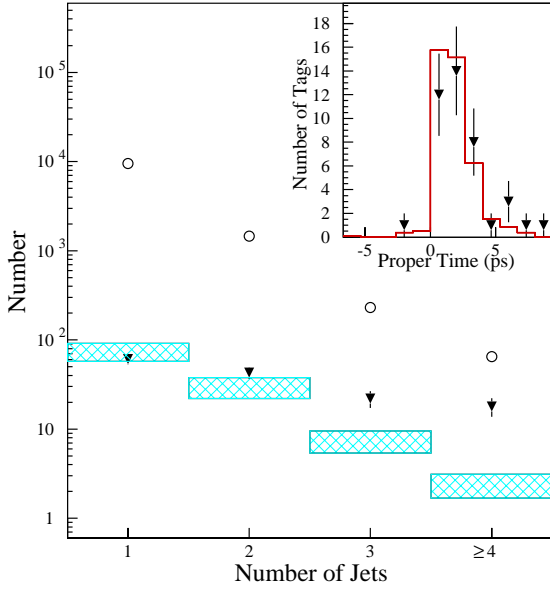


Figure 19: Number of “lepton + jet” events vs. number of jets. Proper decay distance for SVX tagged vertices in $W + \geq 3$ jet events is shown as insert.

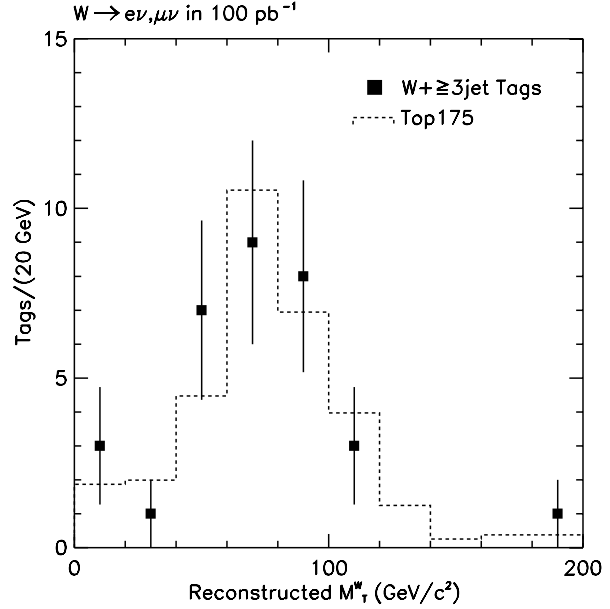


Figure 20: The M_T distribution for the “ $l + \cancel{E}_T$ ” for SVX tagged events vs. Top Monte Carlo.

tagged events (in parentheses) to the backgrounds expected according to the number of jets in the events. A top signal should be in the data with ≥ 3 jets. Both tags show an excess in this channel. The tagging per jet data, rather than the tagging per event data, is used for the significance calculations because it gives better weighting to the events which are double tagged, an effect which is very unlikely for the backgrounds. Figure (19) displays the data before and after the b tagging requirement along with the expected background. The probability of the background fluctuating up to observed signal in the lepton plus ≥ 3 jet channel is 2×10^{-6} and 6×10^{-3} for the SVX tagged and SLT tagged cases, respectively.

There is additional evidence that the excess of events in the ≥ 3 jet channel contains top. The insert in Figure (19) shows the decay lifetime, $c\tau$, distribution for the SVX tags in the $W + \geq 3$ jet sample (as triangles), compared to that expected from b decay in top events (as a histogram) from Monte Carlo. The agreement is quite good. An important kinematic effect would be direct evidence of W 's in the events. This is seen in Figure (20) where the transverse mass of the lepton and neutrino is compared to what W 's from top would produce. Lastly, Figure (21) shows the total transverse energy, the H_T defined earlier, of the SVX tagged events compared to the top Monte

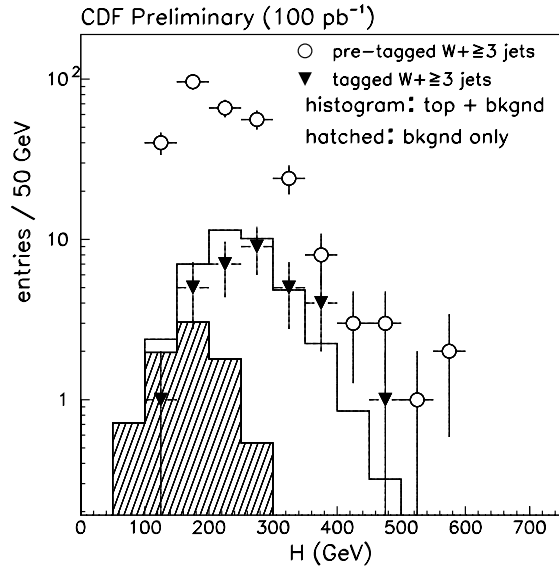


Figure 21: Total transverse energy for pre-tagged and SVX tagged $W + \geq 3$ jet events.

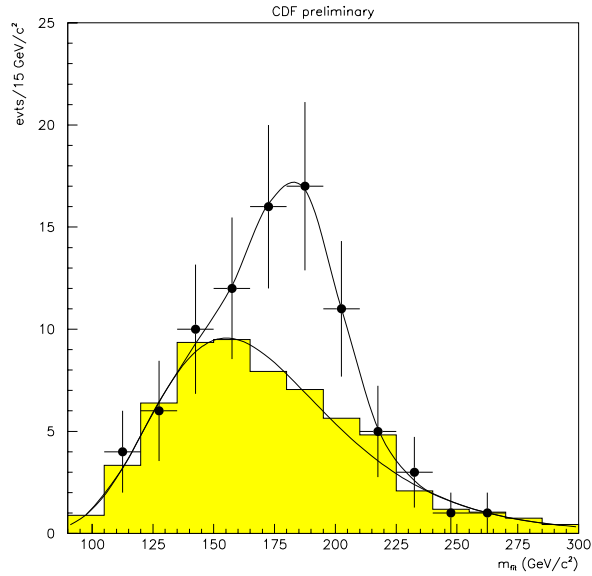


Figure 22: M_{JJ} distribution in All Hadronic Events showing evidence for Top production.

Carlo. All the figures show good agreement with the expectations from top.

3.3. All Hadronic Decay Channel

The channel where both W 's from $t\bar{t}$ decay into two jets was not discussed in previous CDF publications because of the very large backgrounds. Some evidence for top can now be seen in this channel. Including the b quarks there should be 6 jets in this final state. By requiring that at least one jet be SVX tagged and by taking the solution which has the best χ^2 of the ten possible permutations among the 6 leading jets, CDF calculates a mass for a hypothesized top quark in each event. Figure (22) shows the preliminary mass distribution where a clear excess above background is seen in the 160-190 GeV/c^2 region. The number of excess events in the peak is 28 ± 10 which corresponds to a production cross section of 9.6 ± 3.5 pb, where the errors are statistical only.

3.4. $t\bar{t}$ Production Cross Section

From the excess of events in each of the counting experiments CDF can calculate a top quark production cross section. Using 67 pb^{-1} of data and assuming a top quark mass of $175 \text{ GeV}/c^2$ gives $\sigma(t\bar{t}) = 10.9^{+5.9}_{-4.5}$ pb, $6.8^{+2.9}_{-2.3}$ pb and $6.3^{+5.0}_{-4.1}$ pb for the dilepton, SVX and SLT samples, respectively, where the errors are the quadrature combination of

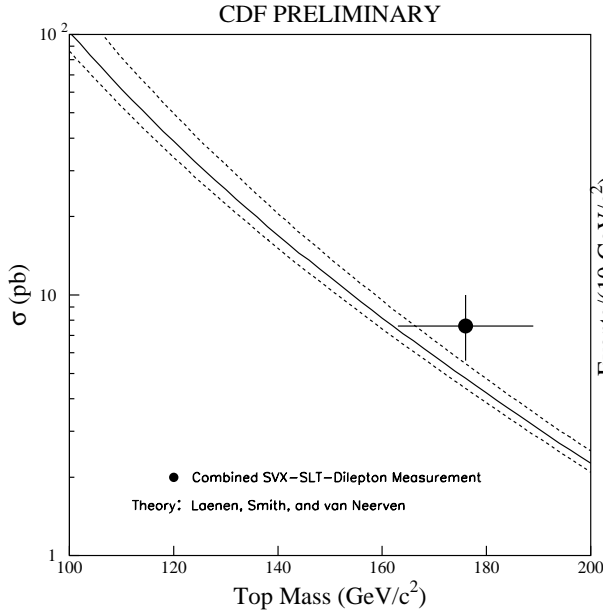


Figure 23: CDF measured cross section for top production vs. theory.

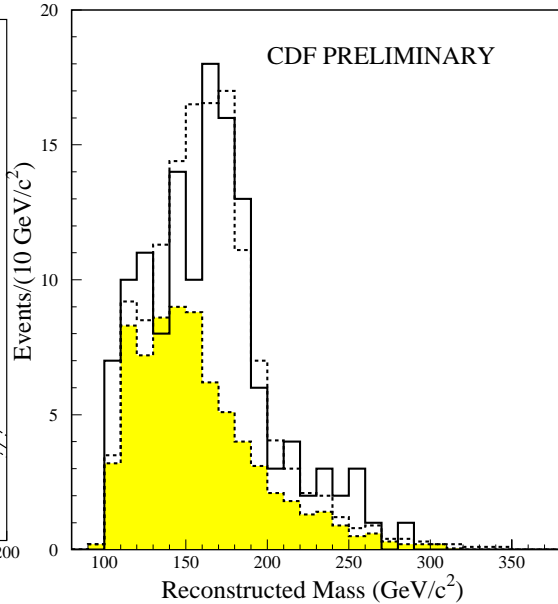


Figure 24: Reconstructed top quark mass for “W + 4 jet” events without any b tagging. Background only is shaded. Background plus top Monte Carlo is dashed histogram.

the statistical and systematic errors. Combining these gives $\sigma(t\bar{t}) = 7.6_{-2.0}^{+2.4}$ pb. Figure (23) shows that this cross section is in good agreement with recent theory.²¹

The full 100 pb^{-1} data set has not been used to calculate a cross section yet. However, assuming the cross section quoted above the expected number of events would be 31.3, 32.8 and 10.4 in the dilepton, SVX and SLT channels whereas the numbers actually observed in the full sample are 32, 36 and 9. The close agreement indicates that the cross section which will come from the 100 pb^{-1} data set will be very close to the present value.

3.5. Determination of the Top Quark Mass

The mass of the top quark can be determined by reconstructing events with a lepton and 4 jets using kinematic constrained fitting techniques. Starting with 296 lepton plus ≥ 3 jet events and requiring that there be a fourth jet with $E_T > 8 \text{ GeV}$ and $|\eta| < 2.4$ leaves 132 events, 32 having a b tag. There are multiple solutions with differing jet assignments, even when the tagged jet is constrained to be a b jet. For each event the top mass of the solution with the best χ^2 is chosen.

This mass analysis gives additional evidence for the top quark if a mass peak appears above the distribution expected from background processes. Figure (24) gives

the mass distribution for all events, without a b tag requirement. An excess above background is seen in the 160 to 190 GeV/c^2 region. The distribution is consistent with 40% $t\bar{t}$ signal with $M_{top} = 175 \text{ GeV}/c^2$ and 60% W +jets background. Figure (25) shows the mass distribution for the 32 b tagged events, where the b tagged jets are constrained to be the b jets in the fitting. A maximum likelihood analysis finds the best top mass to be $M_{top} = 176 \pm 8 \pm 10 \text{ GeV}/c^2$.

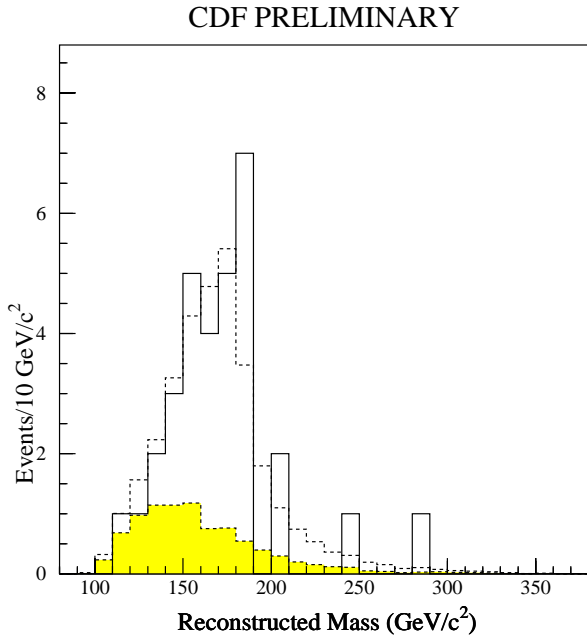


Figure 25: Reconstructed top quark mass for “ $W + 4$ jet” events with b tagging. Background only is shaded. Background plus top Monte Carlo is dashed histogram.

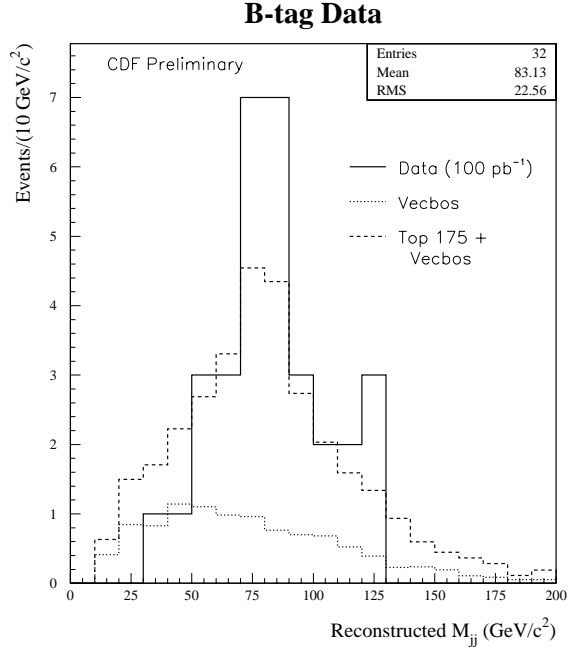


Figure 26: M_{JJ} for jets assigned to W in top analysis.

3.6. Search for Hadronic W Decay in $W+4$ Jets.

Further evidence of top production in these data samples can be established by reconstructing the W mass from its decay into two jets. Two techniques are displayed here. 1) Remove the W mass constraint in the $W \rightarrow jj$ fit and plot the invariant mass for the jet pair assigned to the W decay by the fitter. 2) Plot the invariant mass of the two untagged jets in the double b -tagged $W + \geq 4$ jets. Figures (26) and (27) show the results of these two techniques. Both show clear excesses over the background in the W mass region.

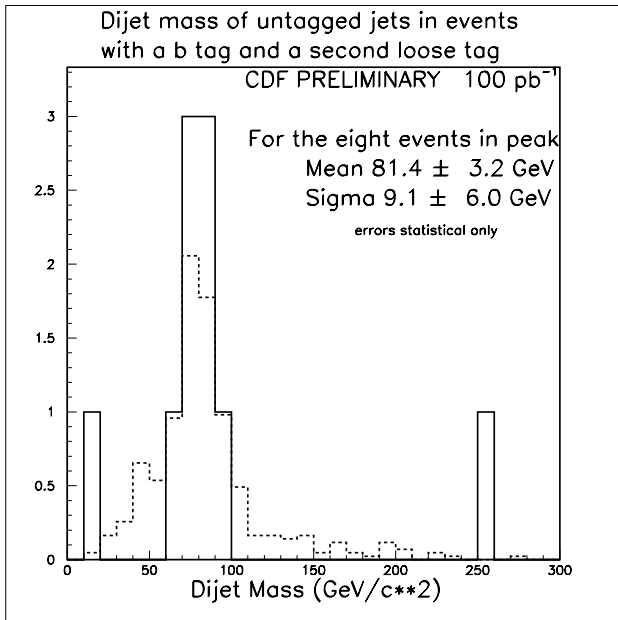


Figure 27: M_{JJ} for untagged jets in the double tagged top events.

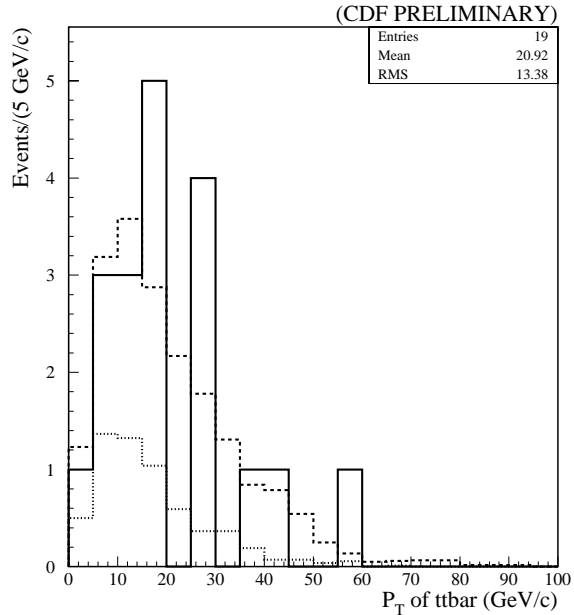


Figure 28: The transverse momentum, P_T , of the $t\bar{t}$ system in b tagged events.

3.7. Properties of the $t\bar{t}$ System

Having unambiguously established the existence of the top quark, the properties of its production and decay become the interesting questions. Evidence for non-standard resonance production of $t\bar{t}$ could be sought by examining the properties of the $t\bar{t}$ system. Figure (28) shows the net transverse momentum and Figure (29) shows the invariant mass of the fitted $t\bar{t}$ pair. Although there is an interesting excess in the $M_{t\bar{t}}$ plot around $525 \text{ GeV}/c^2$, neither plot shows any statistically significant anomaly and both are consistent with the expected behavior for SM top production.

Another method to look for new physics is to measure the $t \rightarrow Wb$ branching ratio. This is supposed to be 100% in the Standard Model. By comparing the number of singly b tagged to doubly b tagged events CDF measures $\frac{Br(t \rightarrow Wb)}{Br(t \rightarrow Wq)} = 0.94 \pm 0.27 \pm 0.13$ in good agreement with the SM.

4. Physics Beyond the Standard Model

CDF has looked for evidence of particles beyond the Standard Model via many methods. Here will be presented searches in three broad categories: 1) supersymmetry, 2) new heavy gauge bosons, i.e. W' and Z' , and 3) other exotics like leptoquarks, composite fermions and technicolor.

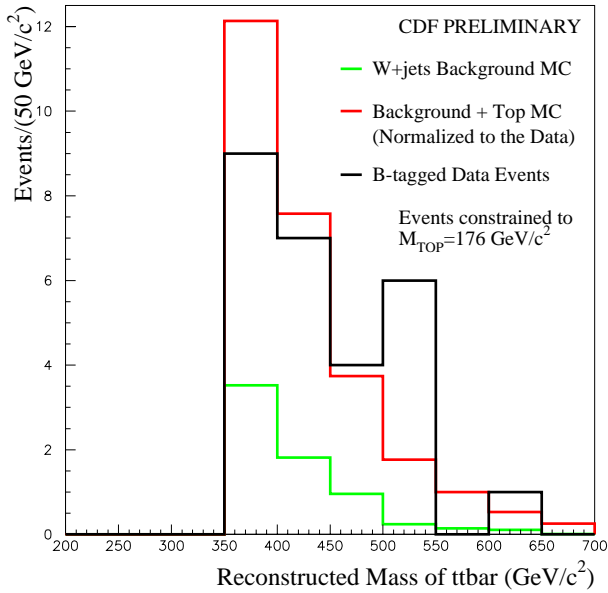


Figure 29: The invariant mass, $M_{t\bar{t}}$, of the $t\bar{t}$ system in b tagged events.

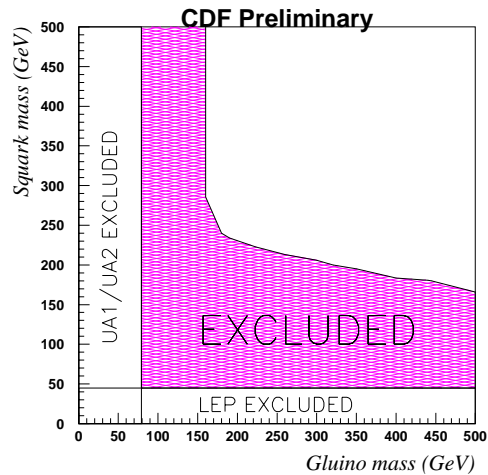


Figure 30: $M_{\tilde{q}}$ vs. $M_{\tilde{g}}$ excluded region

4.1. Supersymmetry

CDF uses two different approaches to look for supersymmetric particles.²² One method looks for “trilepton events” while the second looks for multiple jets plus a large missing energy, \cancel{E}_T , from the unidentified lightest supersymmetric particle, LSP, assumed to be a neutralino.

The trilepton search method looks for three leptons (e and/or μ) in the final state. These would result from the production of chargino-neutralino pairs, $p\bar{p} \rightarrow \tilde{\chi}_1^\pm \tilde{\chi}_2^0$, which decay into one or two high energy leptons and a lightest supersymmetric particle (LSP), which is assumed to be a neutralino, i.e. $\tilde{\chi}_1^\pm \rightarrow l \nu \tilde{\chi}_1^0$ and $\tilde{\chi}_2^0 \rightarrow l l \tilde{\chi}_1^0$. In the search one lepton was required to have $E_T > 11$ GeV (e) or $P_T > 11$ GeV/c (μ) while the other two had to have $E_T > 5$ GeV (e) or $P_T > 4$ GeV/c (μ) plus some other cuts. No events survived all the cuts. This method excluded charginos with mass below about 46 GeV for $\mu = -400$ GeV/c², similar to the LEP limit. The multiple jets plus large \cancel{E}_T search method assumes that if squarks and gluinos are pair produced they will decay into quarks, gluons and LSPs. The minimum \cancel{E}_T requirement needs to be set fairly high, $\cancel{E}_T > 50$ GeV, to avoid backgrounds from, for example, “Z + n jets” and “W + n jets”. CDF rules out at 95% C.L. those parts of MSSM parameter space which predict a detected cross section greater than 1.4 pb passing all cuts. The region of $M_{\tilde{q}}$ vs. $M_{\tilde{g}}$

Dilepton mass distributions (CDF preliminary)

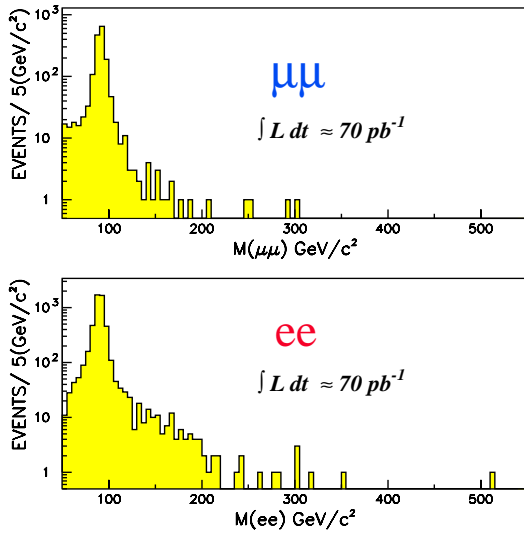


Figure 31: Dilepton (e^+e^- , $\mu^+\mu^-$) invariant mass distributions for Z' search.

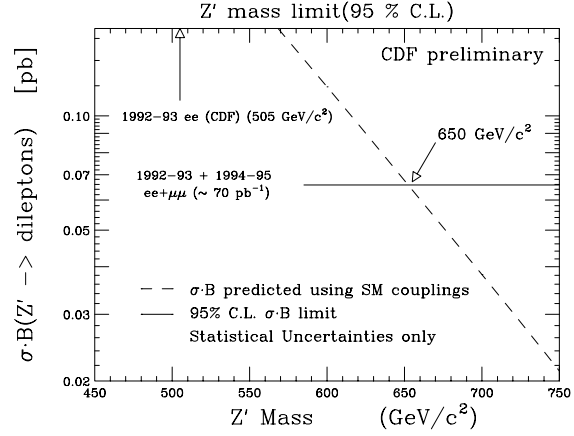


Figure 32: Limit on $Z' \rightarrow l^+l^-$ cross section vs. mass.

space excluded is shown in Figure (30). The parameters associated with this plot are $\tan(\beta) = 4$, $\mu = -400 \text{ GeV}/c^2$, $M_H = 500 \text{ GeV}/c^2$ and $M_{\tilde{t}} = 350 \text{ GeV}/c^2$. For arbitrary $M_{\tilde{q}}$ the data require $M_{\tilde{g}} > 160 \text{ GeV}/c^2$, and if $M_{\tilde{g}} = M_{\tilde{q}}$ then $M_{\tilde{g}} > 220 \text{ GeV}/c^2$.

4.2. New Gauge Bosons

Many theories beyond the Standard Model include an extended gauge group with additional neutral and charged bosons, i.e. Z' or W' . CDF looks for Z' 's as peaks in the dilepton (e^+e^- , $\mu^+\mu^-$) invariant mass distribution, as displayed in Figure (31) for 70 pb^{-1} . The absence of any peaks above γ/Z production allows a 95% CL limit to be set at $650 \text{ GeV}/c^2$ as shown in Figure (32) by assuming Standard Model couplings.

To search for new W' particles one must specify the decay mode. If one assumes that the W' decays with the same branching ratios as the W into $e\nu$ and $\mu\nu$, then the presence of W' would be seen as an excess of events on the high mass tail of the W transverse mass distribution. This could occur for a right handed W' , for example. Figure (33) shows the CDF distribution for the $W' \rightarrow e\nu$ search. Figure (34) shows the CDF limit on σB versus theory. The 95% CL mass limit is $M_{W'} > 652 \text{ GeV}/c^2$ for this decay mode.

If, on the other hand, the decay mode $W' \rightarrow WZ$ is allowed, e.g. for a left handed W' , then the branching ratio for this decay becomes 100% for large W' masses. For this case CDF searches for events with real W 's and Z 's, where $W \rightarrow e\nu$ and $Z \rightarrow q\bar{q}$. Such events would have a high P_T electron, \cancel{E}_T , and two jets with dijet mass near the

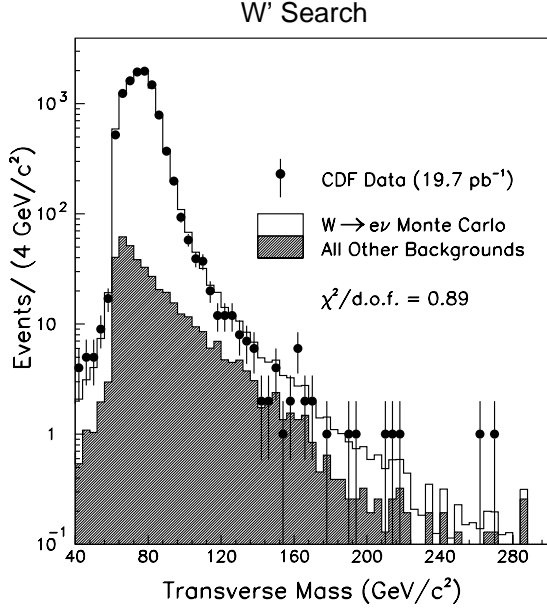


Figure 33: $e\nu$ transverse mass distribution for W' search.

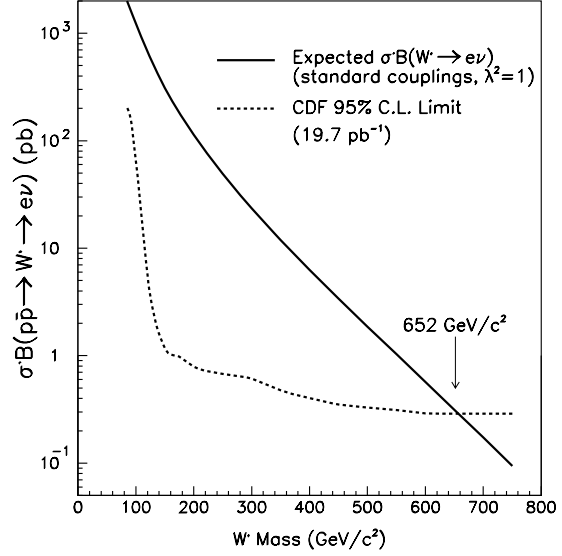


Figure 34: $\sigma B(pp \rightarrow W' \rightarrow e\nu)$ 95% CL limit.

Z mass. Figure (35) shows (W + dijet mass) distribution, and Figure (36) compares the CDF $\sigma \cdot B$ limit versus theory. CDF excludes $205 < M_{W'} < 400 \text{ GeV}/c^2$ at the 95% CL.

4.3. Other Exotic Particle Searches

Two other searches will be described below. The first is searches for leptoquarks, i.e. particles which decay to a lepton plus quark because they carry both baryon and lepton number. These can be classified into generations according to whether they decay into a quark plus electron, muon or tau. The second is searches for new particles which decay into a $q\bar{q}$ pair and, hence, produce two jets. This search looks for bumps in the invariant jet-jet mass distribution, M_{jj} .

4.3.1. Search for Leptoquarks

The CDF limit on the first generation leptoquark comes from only 4.05 pb^{-1} of data.²³ The process is $p\bar{p} \rightarrow L\bar{L} \rightarrow e^+ \text{ jet } e^- \text{ jet}$. Electrons and jets must have $E_T^{e,j} > 20 \text{ GeV}$. If a first generation leptoquark exists its production cross section and decay branching ratio, β , into ($e + \text{jet}$) as opposed to ($\nu + \text{jet}$) must be $\sigma\beta^2 < 55(4.0) \text{ pb}$ at 95% CL for $M_{LQ1} = 45(125) \text{ GeV}/c^2$. The excluded mass regions would be $M_{LQ1} < 116 \text{ GeV}/c^2$ for $\beta = 100\%$ or $M_{LQ1} < 85 \text{ GeV}/c^2$ for $\beta = 50\%$.

Tevatron experiments, unlike e-p collider experiments, can produce second or third generation leptoquarks. CDF has searched for both of these. The second genera-

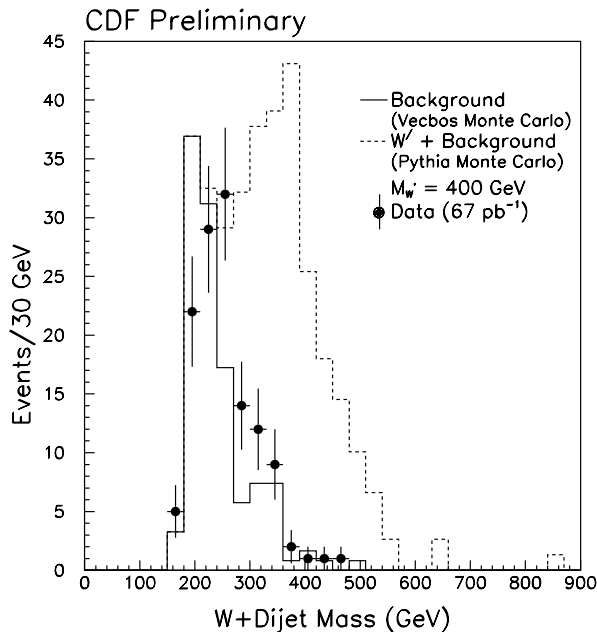


Figure 35: W + dijet invariant mass.

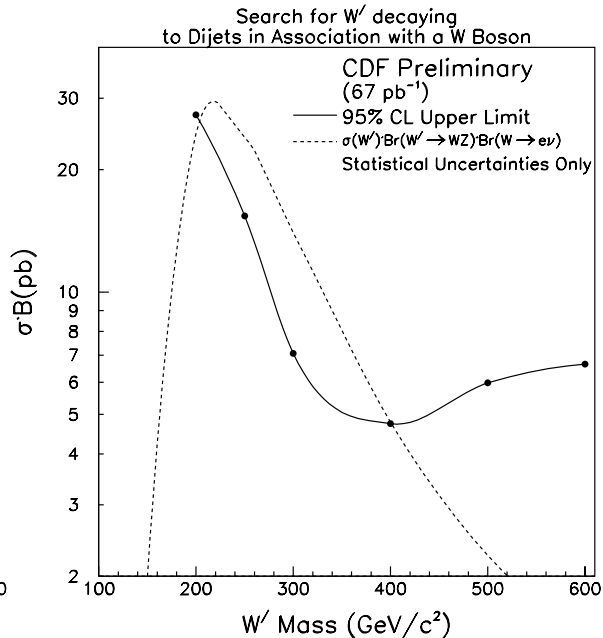


Figure 36: $\sigma B(W' \rightarrow WZ)$ 95% CL upper limit vs. $M_{W'}$.

tion search, μq , results are discussed here, but the third generation search, τq , is still too preliminary for discussion. Figure (37) shows the CDF second generation leptoquark 95% CL upper limits on the production cross section times branching ratio for $LQ_2 \rightarrow \mu + q$ versus mass along with the theoretical prediction. The excluded mass region is $M_{LQ_2} < 180 \text{ GeV}/c^2$ for $\beta = 100\%$ and $M_{LQ_2} < 141 \text{ GeV}/c^2$ for $\beta = 50\%$.

4.3.2. Dijet Bump Hunting

CDF has extended its original search²⁴ for new particles with a narrow natural width decaying into dijets, particles such as axigluons, excited quarks, technirhos, diquarks, etc.²⁵ Using four different triggers CDF observes dijet mass spectra for masses above 150, 241, 292 and 388 GeV/c^2 for integrated luminosities 0.089, 1.92, 9.52 and 69.8 pb^{-1} respectively. The two highest P_T central jets are used to calculate the invariant mass M_{jj} . Figure (38) presents the dijet mass distribution and shows the data to be systematically higher than a PYTHIA prediction. By fitting the data to a smooth function CDF looks for local fluctuations or bumps. No fluctuations are found which are statistically significant. Including systematic uncertainties CDF obtains the 95% CL upper limit on the cross section for new particles shown in Figure (39). Figure (40) shows the excluded mass regions along with some previous searches.

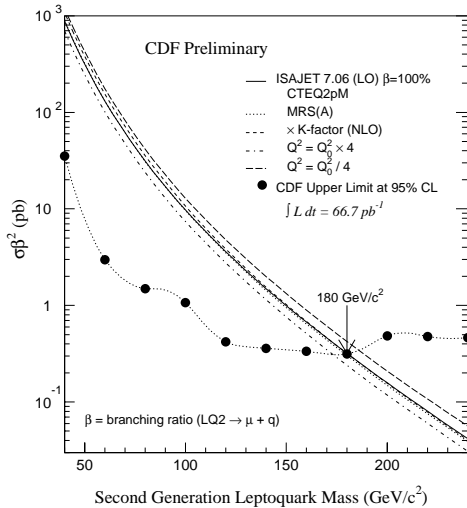


Figure 37: Second generation leptoquark 95% CL upper limit on $\sigma B(LQ_2 \rightarrow \mu + q)$ versus mass.

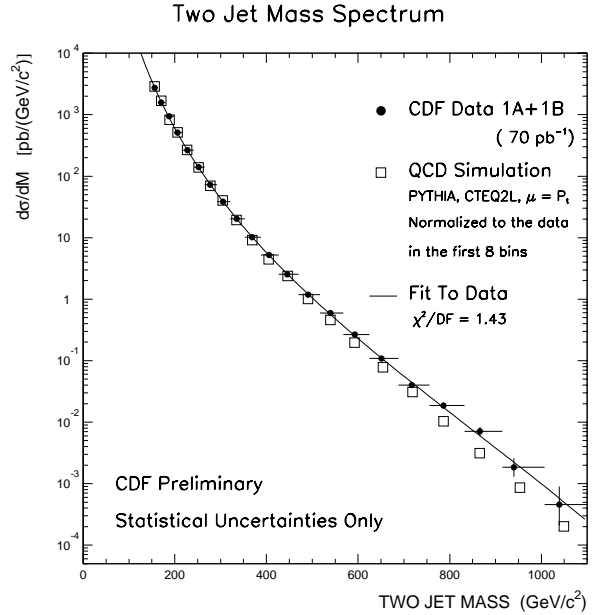


Figure 38: Dijet invariant mass: M_{jj}

5. Electroweak Physics

CDF has a variety of results related to Electroweak phenomena. Measurements of the W and Z cross sections times leptonic branching ratios allow a calculation of the W width and/or lifetime. The measurement of the W mass now has an improved accuracy to $180 \text{ MeV}/c^2$. Diboson production has been examined relative to the Standard Model and anomalous couplings.

All of these studies rely on good W and Z identification. Both identifications generally require an isolated lepton (e, μ) with high P_T . Events with W 's also have a missing transverse energy, \cancel{E}_T , greater than 20 GeV . Events with Z 's require a second, oppositely charged lepton such that the dilepton invariant mass is close to the Z mass.

5.1. Inclusive W and Z cross Sections

From the measurement of the number of W and Z events CDF extracts the product of the production cross section times the leptonic branching ratio $\sigma B(W \rightarrow l\nu)$ and $\sigma B(Z \rightarrow l^+l^-)$ in the e and μ channels.²⁶ These use luminosities of about 19 pb^{-1} . For W 's this gives 2.51 ± 0.08 and $2.48 \pm 0.19 \text{ nb}$ for the e and μ decay, respectively. For Z 's the results are 0.231 ± 0.009 and $0.203 \pm 0.014 \text{ nb}$ for the e^+e^- and $\mu^+\mu^-$ decays, respectively. The Standard Model expectations are 2.42 ± 0.12 and $0.226 \pm 0.010 \text{ nb}$, respectively, in good agreement with the measurements.

Figure 39: 95% CL upper limit on the cross section for new particles.

Figure 40: Excluded mass regions from $X \rightarrow$ dijet search.

5.2. W Width

The W width is determined using the ratios of the above cross sections. These are $R = \frac{\sigma_B(W \rightarrow e\nu)}{\sigma_B(Z \rightarrow e^+e^-)} = 10.90 \pm 0.4$, and $R = \frac{\sigma_B(W \rightarrow \mu\nu)}{\sigma_B(Z \rightarrow \mu^+\mu^-)} = 12.2 \pm 0.8$. CDF takes the electron data, because it is the most accurate, and converts it as $R = \frac{\sigma_W}{\sigma_Z} \frac{\Gamma(W \rightarrow e\nu)}{\Gamma(Z \rightarrow e^+e^-)} \frac{\Gamma(Z)}{\Gamma(W)}$. Using the Z lifetime and partial width into e^+e^- from LEP, the calculated ratio of the W to Z production cross sections, and the Standard Model calculation for the W partial width into leptons produces a W width of $m_W = 2.064 \pm 0.061 \pm 0.059$ GeV. This agrees well with the Standard Model expectation of $m_W = 2.077 \pm 0.014$ GeV.

5.3. W Mass

The direct measurement of the W mass is to date possible only at $p\bar{p}$ colliders. The relations among the masses and couplings of the gauge bosons allow incisive tests of the Standard Model of Weak Interactions. Therefore, one of the most crucial CDF measurements is the W mass.²⁷ This has been done with a precision of about 0.2% which has required extraordinary control of statistical and systematic errors.

The W mass is determined from fits of the $W \rightarrow l\nu$ transverse mass spectra, where “ l ” can be either an electron or muon. The definition of the transverse mass is $(M_T^W)^2 = (E_T^e + E_T^\nu)^2 - (\vec{E}_T^e + \vec{E}_T^\nu)^2$. The transverse energy of the neutrino is not measured directly, but is instead inferred from the energy imbalance in the event. The determination of the momentum and energy scales is crucial for this measurement.

Many checks using the J/ψ , Υ , and Z reconstruction were utilized. A fit using 3268 $W \rightarrow \mu\nu$ events in 19.7 pb^{-1} of data gives $M_W^\mu = 80.310 \pm 0.205 \pm 0.130 \text{ GeV}/c^2$. A fit using 5718 $W \rightarrow e\nu$ events in 18.2 pb^{-1} of data gives $M_W^e = 80.490 \pm 0.145 \pm 0.175 \text{ GeV}/c^2$. The data are shown in Figures (41) and (42) where the arrows indicate the region over which the fitting was performed. Combining these two measurements, accounting for correlated uncertainties, gives $M_W = 80.410 \pm 0.180 \text{ GeV}/c^2$. This precision is a factor of two better than any previous measurement. It agrees with predictions of the Standard Model and indirect measurements from other electroweak results as illustrated in Figure (43).

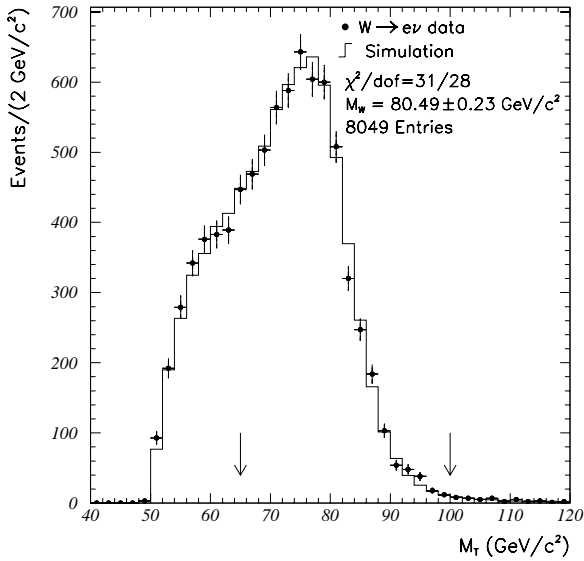


Figure 41: $W \rightarrow e\nu$ transverse mass distribution

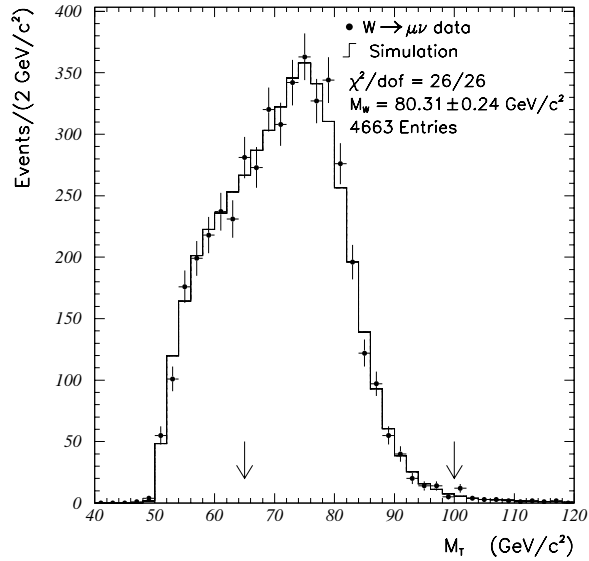


Figure 42: $W \rightarrow \mu\nu$ transverse mass distribution

In the Standard Model the mass of the top quark, W and Higgs are related. This is displayed in Figure (44) which shows the CDF top quark and W masses along with allowed regions for different masses of the Higgs boson. Unfortunately, with the present top quark and W mass resolutions there is little sensitivity to the Higgs mass.

5.4. Anomalous Vector Boson Couplings

As statistics increase CDF is able to begin studying the rare processes of diboson ($W\gamma$, $Z\gamma$, WW , WZ , and ZZ) production.²⁸ In the Standard Model the tri-linear gauge boson couplings give cancellations in the $W\gamma$, WW and ZZ processes but not in $Z\gamma$ and ZZ . Anomalous gauge boson couplings could disrupt these cancellations and produce unitarity violations in cross sections at high energies signaling new physics. Thus, it is important to measure the diboson production cross sections and compare to theory.

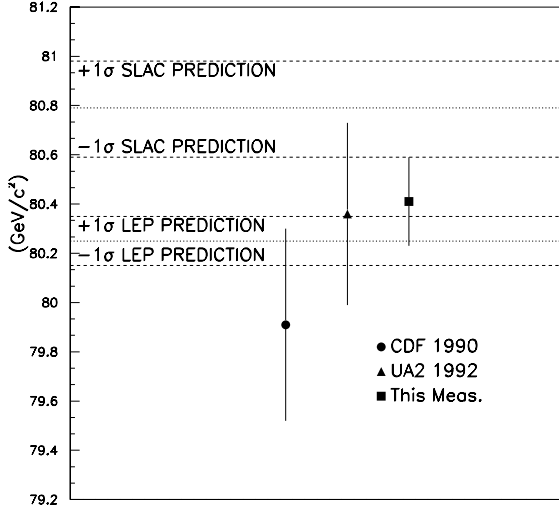


Figure 43: CDF W mass compared to expectations.

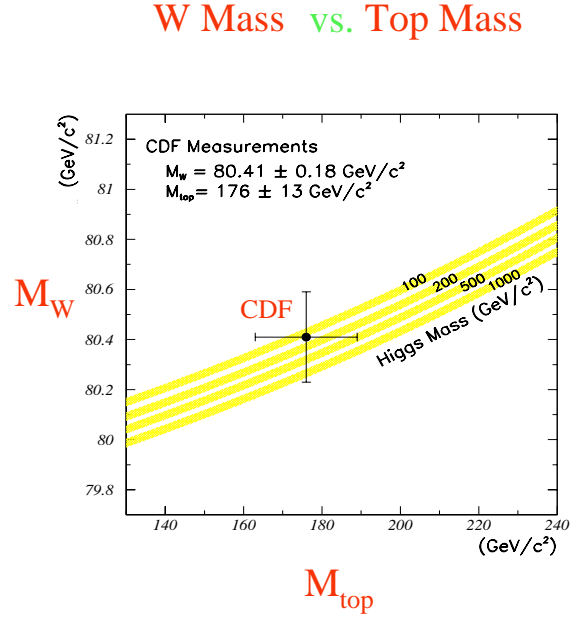


Figure 44: CDF W and Top masses applied to a range of Higgs masses.

5.4.1. $W\gamma$ and $Z\gamma$ Production

Limits on anomalous $W\gamma$ and $Z\gamma$ couplings are set by examining the E_T^γ spectrum for isolated γ 's with $E_T^\gamma > 7$ GeV and $|\eta^\gamma| < 1.1$ and comparing to the Standard Model predictions. CDF has recorded 75(34) $e\nu\gamma$ ($\mu\nu\gamma$) events for 67 pb^{-1} with backgrounds of 16.1 ± 2.4 (10.3 ± 1.2) events which give $\sigma \cdot B(p\bar{p} \rightarrow W\gamma, Z\gamma)$ measurements of 20.5 ± 3.6 (21.5 ± 5.7) pb. The combined $e/\mu \nu\gamma$ value for $\sigma \cdot B$ is $20.7 \pm 2.9 \pm 0.7$ pb which compares well with the SM $W\gamma$ value of 18.6 ± 2.9 pb. Similarly, CDF recorded 18(13) $e^+e^-\gamma$ ($\mu^+\mu^-\gamma$) events for 67 pb^{-1} with backgrounds of 0.9 ± 0.3 (0.5 ± 0.1) which gave $\sigma \cdot B$ measurements of 5.0 ± 1.8 (7.2 ± 2.1) pb. The combined $e^+e^-/\mu^+\mu^-\gamma$ value for $\sigma \cdot B$ is $5.7 \pm 1.4 \pm 0.1$ pb which compares well with the SM $Z\gamma$ value of 4.8 ± 0.6 pb.

The general description of diboson production has two CP conserving couplings (κ, λ) and two CP non-conserving couplings ($\tilde{\kappa}, \tilde{\lambda}$). At the tree level the Standard Model has $\Delta\kappa \equiv (\kappa - 1) = \lambda = \tilde{\kappa} = \tilde{\lambda} = 0$. Because the measured $W\gamma$ and $Z\gamma$ cross sections agree with the SM expectation there is no evidence of anomalous, or CP, coupling. The allowed values are $-1.8 < \Delta\kappa < 2.0$ (if $\lambda = 0$) and $-0.7 < \lambda < 0.6$ (if $\Delta\kappa = 0$).

5.4.2. WW and WZ Production

The signature for non-SM couplings in weak diboson pair production is an excess rate for bosons with high P_T . CDF searched the Run 1A data, $\sim 19 \text{ pb}^{-1}$, for WW and

WZ candidates consistent with a leptonic decay of one boson, $W \rightarrow l\nu$ or $Z \rightarrow ll$, and hadronic, 2 jet, decay of the other. CDF observed one candidate in the $l\nu jj$ channel and none in the $lljj$ channel. The Standard Model predicts 0.13 $WW, WZ \rightarrow l\nu jj$ events and 0.02 $WZ \rightarrow lljj$ events. CDF extracted limits for anomalous couplings by assuming $\Delta\kappa \equiv \Delta\kappa_\gamma = \Delta\kappa_Z$ and $\Delta\lambda \equiv \Delta\lambda_\gamma = \Delta\lambda_Z$. Setting all other couplings to their SM values gives $-0.9 < \Delta\kappa < 1.0$ and $-0.6 < \lambda < 0.7$ for $\lambda_{FF} = 1.5$ TeV and $-1.1 < \Delta\kappa < 1.3$ and $-0.81 < \lambda < 0.84$ for $\lambda_{FF} = 1.0$ TeV.

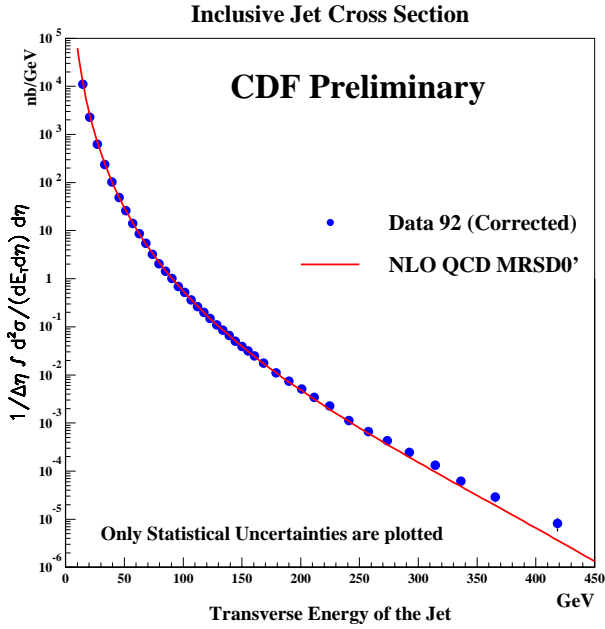


Figure 45: Fully corrected inclusive jet cross section compared to NLO QCD.

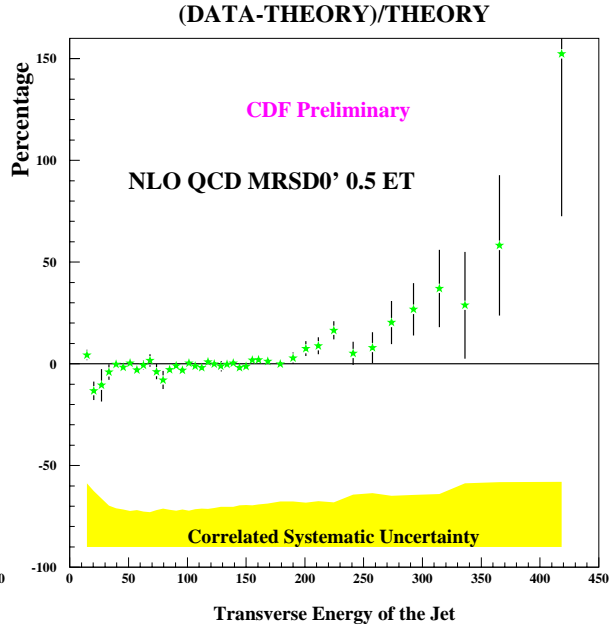


Figure 46: $(\text{Data} - \text{QCD})/\text{QCD}$ for fully corrected inclusive jet cross section.

Another technique for looking for anomalous couplings is to look in the dilepton decay channel of WW . To suppress backgrounds no jets are allowed. In 65 pb^{-1} CDF finds 5 events. This corresponds to a cross section of $\sigma(p\bar{p} \rightarrow WW + X) = 13.8_{-7.9}^{+9.6} \text{ pb}$ in good agreement with the SM value of 9.5 pb.

6. Tests of Quantum Chromodynamics

The strong interaction as encompassed by Quantum Chromodynamics can be studied at CDF through many different channels.²⁹ These include jet production, vector boson production, hard diffraction and rapidity gaps. The discussion here will only address QCD effects in single and multi jet production. The main point will be that there is an apparent excess in the data compared to theory for very high energies in the inclusive and dijet samples.

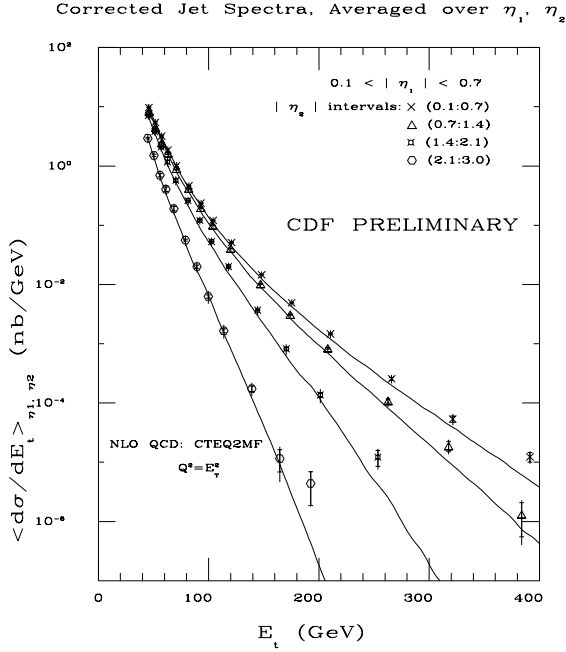


Figure 47: Corrected jet spectra for different rapidity ranges.

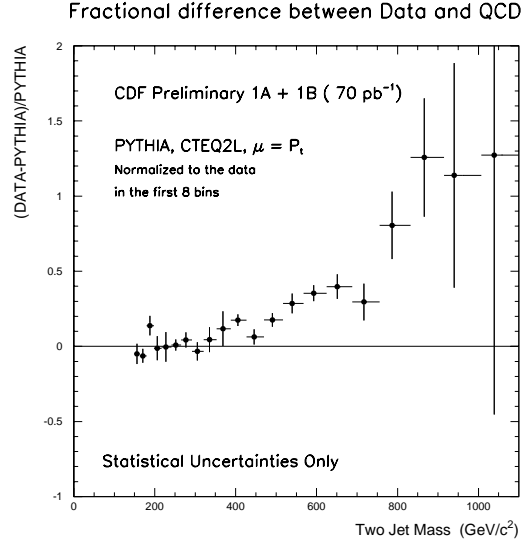


Figure 48: $(\text{Data} - \text{QCD})/\text{QCD}$ for M_{jj}

6.1. Inclusive Jet Cross Section

CDF has made measurements of the inclusive jet cross section out to a transverse energy of about $450 \text{ GeV}/c^2$. The statistical precision is typically a few percent and the systematic errors are about 20-40% depending upon the jet E_T . The NLO QCD calculations³⁰ have very small theoretical uncertainties as well. The measurements probe distance scales in the tail of the distribution in the range of 10^{-17} cm , which are the shortest distances attainable technically. Thus, the inclusive jet cross section is a good place to search for new phenomena.

The present measurement is based upon 19.3 pb^{-1} of data. The data after corrections for detector effects³¹ is shown in Figure (45). Notable cuts are that the cone radius is $R=0.7$ and the jet must have $0.1 < |\eta| < 0.7$. The data are compared to the predictions³⁰ of NLO QCD. They show impressive agreement over seven orders of magnitude. However, above about 200 GeV the data becomes somewhat higher than the theory, as can be seen in Figure (46) by taking the ratio of the difference to the theory: $\frac{(\text{data} - \text{theory})}{\text{theory}}$. This figure also shows the correlated systematic uncertainties which don't change much with E_T . These are still under study. Different parton distributions tend to change the normalization, but not the shape to the extent seen in the figure. There is, of course, the possibility that the deviation is a first hint of new physics of some kind.

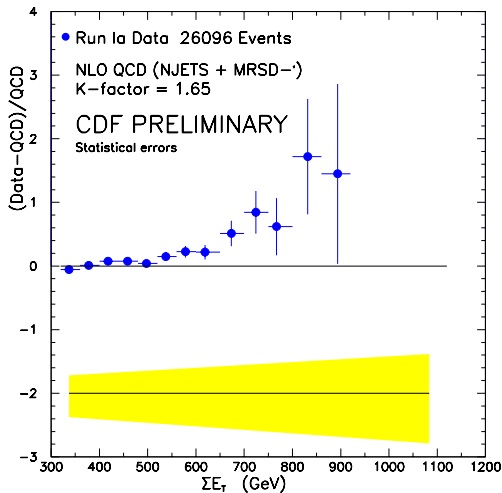


Figure 49: $(\text{Data-QCD})/\text{QCD}$ for fully corrected ΣE_T cross section

6.2. Dijet Production

CDF has examined the dijet production to check the excess production observed in the inclusive jet spectrum. The corrected jet spectra are averaged over small regions of rapidity. The rapidity of one jet is required to be in the range of $0.1 < |\eta| < 0.7$ while the second is taken over various bins. As shown in Figure (47) an excess at large E_T is seen compared to theory for all rapidity ranges.

In the discussion of searches for new particles the point was made that the dijet invariant mass, M_{jj} , distribution exceeded the theoretical expectation from a Leading Order QCD shower Monte Carlo (PYTHIA) program with full CDF detector simulation. This effect is displayed as $\frac{(\text{data-theory})}{\text{theory}}$ in Figure (48). The jets are required to satisfy $|\eta| < 2.0$ and the events are required to have $|\cos(\theta^*)| < 2/3$. There are 70 pb^{-1} of data in the analysis. The QCD prediction is normalized to the data in the mass range of 150-300 GeV/c^2 . There is a significant excess for M_{jj} above about 500 GeV/c^2 .

6.3. ΣE_T Cross Section

Another approach to small distance phenomena is to look at the total transverse energy in the events. This CDF analysis uses 19.3 pb^{-1} of data. The general properties of the ΣE_T cross section are well described by QCD theory³¹ except at the largest ΣE_T as shown in Figure (49). The theory is normalized in the region 320-480 GeV. The figure shows $\frac{(\text{data-theory})}{\text{theory}}$ along with the systematic error estimate. The data is significantly above the theory for $\Sigma E_T > 550 \text{ GeV}$.

7. Future Plans at Fermilab and CDF

There are significant plans for upgrading both the Tevatron and CDF over the next few years. Run II is to begin in 1999 with a two stage improvement. The first increases the CM energy from 1.8 TeV to 2.0 TeV and adds the Main Injector, now under construction, for an increase in instantaneous luminosity by a factor of four. The second stage introduces a new scheme for producing and recycling anti-protons which should produce an increase in luminosity by 2.5. Together these should allow CDF to collect about 1 fb^{-1} of data per year, 20 times better than now.

The CDF detector must be upgraded to keep pace with the luminosity and detector technical advances. The entire charged particle central tracking system will be replaced with 1) a new five-layer silicon vertex detector, SVX II, with 3-D stereo read-out and twice the length of the present SVX', 2) a scintillating fiber tracking system and 3) a straw tube tracker. A scintillating tile and fiber calorimeter will be in the forward region of $1.1 < |\eta| < 3.5$. Improved muon coverage will fill the central region of $|\eta| < 1.0$ and the forward region of $1.5 < |\eta| < 3.2$. There will be new trigger at all levels capable of operating at short bunch spacings (132 nsec). The SVX II will be able to produce impact parameter information at Level 2 which will allow triggering on events containing B decays.

These advances in the accelerator and the CDF detector should continue to produce interesting and exciting physics into the next millennium.

8. Acknowledgements

I thank my CDF colleagues, the Fermilab staff and the technical staffs of the participating institutions for their vital contributions. The CDF work was supported in part by the Department of Energy, the National Science Foundation, the Instituto Nazionale di Fisica Nucleare, the Ministry of Science, Culture, and Education of Japan, and the Alfred P. Sloan Foundation and the Grainger Foundation.

References

1. F. Abe et al., CDF Collaboration, Nucl. Instrum. Methods Phys. Res., A, 271, 387 (1988).
2. D. Amidei et al., Nucl. Instrum. Methods Phys. Res., A, 350, 73 (1994).
3. F. Abe et al., CDF Collaboration, FERMILAB-PUB-95/317-E, Accepted for publication in Phys. Rev. D, April, 1996.
F. Abe et al., CDF Collaboration, FERMILAB-CONF-94/136-E.
F. Abe et al., CDF Collaboration, Phys. Rev. Lett.71, 1685 (1993).
4. V. Canale, Proceedings of the "XXXth Recontres de Moriond", QCD and High Energy Hadronic Interactions, Les Arcs, Savoie, France, March 1995.
5. V. Chernyak, preprint Budker INP 95-18.
M. Shifman, Preprint TPI-MINN-94/32-T.
I. Bigi, preprint UND-HEP-95-BIG06, Proceedings of the 6th International Symposium on Heavy Flavor Physics, Pisa, Italy, June, 1995.
6. F. Abe, CDF Collaboration, Phys. Rev. Lett.75, 1451 (1995).
7. I. Bigi, preprint UND-HEP-95-BIG06, Proceedings of the 6th International Symposium on Heavy Flavor Physics, Pisa, Italy, June, 1995.
I. Dunietz, preprint FERMILAB-PUB-94/361-T.

8. F. Abe et al., CDF Collaboration, Phys. Rev. Lett.74, 4988 (1995).
9. F. Abe et al., CDF Collaboration, Phys. Rev. Lett.69 (1992).
10. E. Braaten, M. Doncheski, S. Fleming, M. Mangano, Phys. Lett. B333, 548 (1994).
M. Cacciari, M. Greco, Phys. Rev. Lett.73, 1586 (1994).
E. Close, "New Metastable Charmonium and ψ' Anomaly at CDF", RAL-94-093, August 1994.
P. Cho, S. Trivedi, M. Wise, "Gluon Fragmentation into Polarized Charmonium", FERMILAB-PUB-94/256-T.
D. P. Roy, K.Sridhar, "A Possible resolution of the CDF ψ' Anomaly", CERN-TH.7434/94, TIFR/TH/94-33, Sept. 1994.
E. Braaten and S. Fleming, Phys. Rev. Lett.74, 3327 (1995).
P.Cho and M. Wise, Phys. Lett. B346, 129 (1995).
11. F. Abe, CDF Collaboration, Phys. Rev. Lett.71, 2537 (1993).
12. E. Braaten, et al, Phys. Lett. B333, 548 (1994)
P. Cho and A.K.Leibovich, CALT-68-1988, May 1995.
13. P.Nason, S. Dawson and R.K. Ellis, Nucl. Phys. B303, 607 (1988); Nucl. Phys. B327, 49, 1989; Nucl. Phys. B335, 260 (1990).
14. C. Peterson, D.Schlatter, I.Schmitt and P.Zerwas, Phys. Rev. D. 27, 105 (1983).
15. M.Mangano, et. al. Nucl. Phys. B373 (1992).
16. A. Ali et al. Proceedings of the ECFA Workshop on the Physic of the European B Meson Factory, 155 (1993).
17. F. Abe, et al, CDF Collaboration, Phys. Rev. D. 50, 2966 (1994).
F. Abe, et. al., CDF Collaboration, Phys. Rev. Lett.73, 225 (1994).
18. F. Abe, et al, CDF Collaboration, Phys. Rev. Lett.74, 2626 (1995).
19. S. Abachi, et al, D0 Collaboration, Phys. Rev. Lett.74, 2632 (1995).
20. F. Abe, et. al., CDF Collaboration, Phys. Rev. D. 51, 168 (1995).
F. Abe, et. al., CDF Collaboration, Phys. Rev. D. 52, 2605 (1995).
21. E. Laenen, J. Smith, & W.L. van Neerven, Phys. Lett. 321B, 254, 1994.
The calculation by Berger and Contopanagos, ANL-HEP-PR-31 (1995), gives a slightly higher cross section and better agreement with the CDF measurement.
22. J.Hauser, Proceedings of the 10th Workshop on Proton-Antiproton Collisions, Fermilab, May, 1995.
H. Baer et al., FSU-HEP-950401.
F. Abe, et al., CDF Collaboration Phys. Rev. Lett.69, 3439 (1992).
23. F. Abe, et al., CDF Collaboration, Phys. Rev. D. 48, R3939 (1993).
24. F. Abe, et al., CDF Collaboration Phys. Rev. Lett.74, 3538 (1995).
F. Abe, et al., CDF Collaboration Phys. Rev. Lett.71,2542 (1993).
25. R. Harris, Proceedings of the 10th Workshop on Proton-Antiproton Collisions, Fermilab, May (1995).
26. F. Abe, CDF Collaboration, Fermilab-Pub-95-301-E(1995), submitted to PRD.
F. Abe, et. al., CDF Collaboration, Phys. Rev. Lett.73, 220 (1994).
F. Abe, CDF Collaboration, Phys. Rev. D. 52, 2624 (1995).
27. F. Abe, et. al., CDF Collaboration, Phys. Rev. D. 52, 4784 (1995).
28. F. Abe, et.al., CDF Collaboration, Phys. Rev. Lett.74, 1936 (1995).
F. Abe, et. al., CDF Collaboration, Phys. Rev. Lett.74, 1941 (1995).
F. Abe, et. al., CDF Collaboration, Phys. Rev. Lett.75, 1017 (1995).

29. E. Buckley-Geer, CDF Collaboration, Fermilab-Conf-95/316-E, Proceedings International Europhysics Conference on HEP, Brussels, Belgium, 1995.
30. S. Ellis et al., Phys. Rev. Lett.62 2188 (1989). Phys. Rev. Lett.64. 2121 (1990)
F. Aversa et al., Phys. Lett. B210, 225 (1988). Phys. Lett. B211, 465 (1988). Nucl. Phys. B327, 105 (1989).
W. Giele et al., Nucl. Phys. B403, 633, (1993).
31. F. Abe et al, CDF Collaboration, Phys. Rev. Lett.70, 608 (1995).